Engineering Structures 318 (2024) 118599

Contents lists available at ScienceDirect

Engineering Structures

journal homepage: www.elsevier.com/locate/engstruct

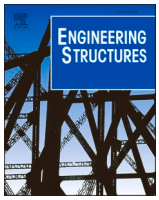

Innovative demountable steel-timber composite (STC) beams: Experimental full-scale bending tests

Alfredo Romero *, Christoph Odenbreit

ArcelorMittalChair of Steel Construction at the University of Luxembourg, L-4365 Esch-sur-Alzette, Luxembourg

ARTICLE INFO

Keywords:
Bending test
Design for disassembly
Industrialized construction
Prefabricated construction
Steel-timber composite (STC) structures
STC beam

ABSTRACT

This study introduces an innovative demountable steel-timber composite (STC) flooring system with potential for reuse. The flooring system consists of downstanding hot-rolled I-shaped steel profiles and laminated veneer lumber (LVL) slabs connected to the steel beams with novel shear connectors. This STC flooring system aimed at reducing embodied carbon and optimizing the use of resources, offer an alternative to traditional, carbon-intensive flooring systems. The novel shear connections implemented in the STC beams facilitate demountability, adaptability, reconfiguration, and relocation of structural components, aligning with circular economy principles. Moreover, this flooring system exhibits significant promise for modularization, standardization, and off-site serial production, making it ideal for prefabrication in standard sizes and modules. Two full-scale STC beams, each with a span of 10 m, an LVL slab width of 2.51 m and thickness of 144 mm connected to a steel profile IPE 400, were simply supported and tested in six-point bending to assess their flexural response. The two tested beams were identical in terms of geometry, materials, and shear connection distribution, but differed in the type of shear connection implemented. This contribution outlines the details of the innovative flooring system and the novel connections that enable demountability and reusability of the components. Specifics of the two STC beam specimens, their assembly, the test setup, the instrumentation, and the testing procedure are presented. The results of the two full-scale bending tests demonstrate their significant load-bearing and deformation capabilities as well as potential for reuse. Additionally, the results indicate the efficacy of the novel shear connections and the beams' overall structural integrity. Despite the extensive deformation of the STC beams, the shear connections remained undamaged and slip values of less than 7 mm were recorded in the last loading stages. Within the elastic range, maximum slip values of less than 1 mm were recorded, highlighting the structural components' potential for reuse. Midspan deflections exceeding $\ell/20$ demonstrate good ductility. Strain measurements on the timber slabs revealed that the slabs' width was not fully utilized, leading to the determination of an effective width of $\ell/5.5$.

1. Introduction

In response to the urgent need for alternatives to non-sustainable construction practices, steel-timber composite (STC) structures have shown the potential to be a solution that is efficient and sustainable. In particular, the interest in STC flooring systems incorporating timber engineered products such as cross-laminated timber (CLT) and laminated veneer lumber (LVL) has increased due to their reduced environmental impact compared to other construction materials [1–3].

The interest and research on STC beams and flooring systems has increased in the last years. Research in this domain includes the study of the shear connections' behaviour, the load-deformation response and capacity of STC beams and joints, long term effects, vibrations, and the diaphragm behaviour.

Shear connections for STC beams implementing screws, bolts, C-type connectors, epoxy adhesives, steel plates (both punched and embedded in the timber), combinations of these methods, and mechanical connectors embedded in grout pockets, have been the focus of dedicated research efforts. These studies, which include both static [4–22] and cyclic [23–25] push-out tests as well as numerical simulations, have provided comprehensive insights into the connections for STC beams. Asiz and Smith investigated the load-deformation behaviour of screws connecting steel beams and CLT panels, finding that their capacity was adequate for use in flooring systems. Loss et al. [5,23] did static and

* Corresponding author.
E-mail address: alfredo.romero@uni.lu (A. Romero).

https://doi.org/10.1016/j.engstruct.2024.118599
Received 12 December 2023; Received in revised form 13 March 2024; Accepted 10 July 2024
Available online 31 July 2024

cyclic push-out tests to study the mechanical behaviour of steel beam to CLT panels connections, including connections with screws, bolts, c-type connectors, glue, combinations of these connectors, and steel plates embedded in timber with epoxy resin. Based on the results, two connections (i.e. inclined screws and plates embedded in epoxy resin) were selected for their implementation in STC floors due to their simplicity and ease of installation, as well as good load-bearing and deformation capacities. Hassanieh et al. [6–10] did static push-out tests to study steel-to-timber (i.e. LVL and CLT) connections using bolts, screws, glue and screws, screws with punched metal plates and bolts embedded in grout pockets. Results indicate that the orientation of the grain of the panels significatively influences the response and capacity of the connections. Screws and bolts showed good deformation and bearing capacity, their capacity was enhanced with the implementation of punched metal plates, and the connections with glue exhibited high stiffness and load-bearing capacities but were associated to brittle failure with limited deformation capacity. The bolts in grout pockets showed the largest load-bearing capacity. Furthermore, numerical models were developed to replicate the push-out tests and conduct parametric studies to investigate the influence of different parameters on the response of the connections. Yang et al. [11] carried out static push-out tests on connections of steel beams and glulam plates using bolts and screws, connections with screws showed the largest stiffness but bolted connections exhibited better ductility and load-bearing capacity. Wang et al. [12] assessed steel-to-glulam connections with inclined screws using special taper washers, the capacity of these connections was higher than the capacity of vertical screws due to the use of longer screws that increase the embedment depth. Zhao et al. [13] investigated connections with screws with a portion of the tip embedded in grout pockets, finding that the stiffness and strength of these connections is improved when compared to connections with only screws. Moritani et al. [14] conducted tests to analyse connections between cold-formed steel (CFS) beams and CLT panels. Five connectors were studied, including screws, bolts and bolts with T-nuts and threaded inserts. The connections exhibited good deformation capacity, bolted connections with T-nuts, and connections with both, threaded inserts and T-nuts, had the best performance in terms of strength. Gao et al. [15] executed static push-out tests to investigate the response of steel-to-timber connections with bolts and screws. Bolts had the best strength and stiffness, and it was determined that the strength and stiffness of the connections increase with increasing thickness of the timber. Chybinski and Polus [16,17] studied bolted connections and connections with screws reinforced with C-type connectors (i.e. bulldog and geka) used to connect LVL and aluminium beams, it was concluded that bulldog and geka connectors improve the strength of the connections but have negligible effects on their stiffness. Similarly, Zhou et al. [18] assessed aluminium-to-timber (i.e. glulam) connections with bolts and screws, their load-slip behaviour and capacity was similar to connections implementing steel beams. Shear studs embedded in grout to connect CLT panels and steel beams have been investigated numerically by Zhang and Ling [19] and experimentally by Böhm [22] who also studied steel-to-timber connections with inclined screws. The screws were set at a skew angle of 45° relative to the vertical axis, and their orientation across various skew angles relative to the horizontal plane was investigated to assess their impact on the behaviour and load-bearing capacity of the connection. It was discovered that the load-bearing capacity decreases as the skew angle in the horizontal plane increases. Conversely, the capacity is significantly enhanced with an increase in the length of the screws. Ataei et al. [24,25] evaluated the response of connections with screws, bolts and bolts in grout pockets under cyclic loading, the results of the tests indicate that the connections have high ductility and energy dissipating capacity, larger than the minimum requirements established in design codes (e.g. EN 1998–1 [26]).

Current research on STC beams and flooring systems, which includes both bending tests and numerical simulations [27–32], has largely been centred around steel beams connected to CLT slabs, primarily using screws as shear connectors. To date, only a few bending tests have been reported in the literature on STC beams that implement LVL slabs, CLT slabs, and glulam slabs. Furthermore, these studies typically involved timber slabs of narrow width connected to hot-rolled steel beams, without investigating the shear lag effect. The literature lacks studies addressing shear lag effects in these configurations, as well as on defining an effective width for the analytical determination of the bending capacity of STC beams. Asiz and Smith [27] studied numerically the response to seismic and wind loads of medium-rise and high-rise buildings with steel frame and CLT floors, the drifts were compared with those obtained for buildings with the same steel frame but with concrete floors, results indicate that the drifts are significantly smaller for buildings with timber slabs. Hassanieh et al. [28,29] carried fourteen 4-point bending tests on STC beams with LVL (seven tests) and CLT (seven tests) slabs implementing bolts, screws, and screws with glue. It was determined that the stiffness of beams with bolted connectors was higher than the stiffness of beams with screws, in general, the beams showed ductile behaviour, except the STC beams with screws and glue, which were associated to brittle failure. Furthermore, from these bending tests, only two of these implemented bolted connections, one STC beam with LVL slab and one with CLT slab. In these two tests, the full preload of the bolt was not reached, and damages were observed in the LVL due to compression of washers against the slab exerted by the preload of the bolt. Loss and Davison [30] conducted 6-point bending tests on modular prefabricated STC floor components consisting of CFS beams connected to CLT panels, implementing two types of connections: inclined screws (three tests) and steel plates embedded in timber with epoxy resin (three tests). The beams were tested under (i) simply supported conditions and (ii) restraining the rotation of the supports. It was observed that both tested systems — inclined screws and steel plates — performed similarly in terms of bending capacity and initial stiffness. Furthermore, the study found that restraining the rotation of the supports resulted in increased load-bearing capacity and stiffness of the floor components. A similar STC floor component combining steel plates embedded in timber and vertical screws was tested in 6-point bending and a numerical model was developed to replicate the test [31]. The results demonstrate adequate stiffness and bending capacity of the STC floor module, and a high level of composite action. Zhao et al. [33] used screws, alone and with their tips anchored in pockets filled with either mortar or epoxy resin, to connect glulam slabs to hot-rolled I-shaped steel beams. They conducted 4-point bending tests to analyse the flexural response of the STC beams. The test results showed that the connections involving screws with their tips anchored in mortar-filled pockets or epoxy resin demonstrated increased stiffness and strength compared to those using screws alone. The study concluded that mortar was more effective than epoxy resin in enhancing bending stiffness and strength. Böhm et al. [32] carried out fifteen 4-point bending tests on STC beams with CLT slabs and I-shaped hot-rolled steel profiles, analysing spans of 8.1 m and 10.8 m, connected with inclined screws and shear studs in grout pockets. Results showed adequate deformation capacities of the STC beams, suggesting that their design is likely to be governed by serviceability limitations (e.g. deflection and vibration) rather than bending capacity. The beams implementing screws showed larger stiffness than the beams with shear studs in grout pockets, additionally, screws were more effective to limit slip. Furthermore, in the beams with shear studs in grout pockets there was a significant loss of stiffness due to the mortar cracking at about 30 % of the maximum load.

STC beams have been also studied analytically and numerically [30, 34–39], the analysing methods consist on the implementation of the g-method [40,41], the use of the elastic theory of layered beams, full plastic analyses with rectangular stress blocks similar to Eurocode 4 [42] procedure for SCC beams, and the implementation of strain-controlled approaches. Results have been compared with experimental and numerical results, showing good agreement for most cases. However, it remains unclear which effective width has to be considered in the

analyses of beams with wider timber slabs than those tested and reported in the literature.

Research has also focused on the load-deformation behaviour and capacity of STC joints, using tests and numerical models to develop analytical formulations to estimate their capacity [43–52]. Long-term effects under sustained loads have been examined experimentally and numerically on STC joints, as well as on STC beams and their shear connections [53–57]. Additionally, experimental and numerical modal analyses, as well as human-induced vibration tests, have been conducted to asses vibrations in STC beams and slabs [32,58–67]. The diaphragm behaviour has been analysed through experimental and numerical methods [23,68–70]. Investigations into the sustainability potential have also been conducted [1,71]. Hybrid frames combining timber-timber composite (TTC) floor panels and steel columns have been also investigated, Hammad et al. [72] conducted a comprehensive investigation on the response of the TTC-to-steel column joints. Different engineering products were used (e.g. CLT, LVL, GLT), and the influence of different parameters was investigated.

Building upon this foundation of research, the practical advantages of the STC structural system are significant and include: (i) enhanced strength and stiffness compared to hybrid non-composite systems, leading to (ii) the possibility to create larger open spaces; (iii) lighter construction compared to other structural solutions (e.g. concrete and steel-concrete composite floors), which results in (iv) benefits for the foundations, column sizes and the dynamic response of the building; (v) potential reductions in construction time and costs due to the feasibility of prefabrication and modularisation, (vi) lower embodied carbon, and (vii) the potential for disassembly.

The environmental benefits of STC systems can be amplified when they are designed for disassembly and reusability. Demountable systems facilitate the recovery and reuse of structural elements, thereby extending their lifecycle, minimizing waste, and reducing the demand for raw materials and energy associated with manufacturing new components. Furthermore, designing for disassembly and reuse of all structural components contributes to transitioning the construction sector towards a circular economy. This approach aligns with the ambitious carbon neutrality goals set by policies like the European Green Deal [73] and supports the efficient and responsible use of resources, a core principle of the United Nations' Sustainable Development Goals [74]. Besides the environmental benefits of demountable and reusable systems, there are also potential economic advantages, for instance, the costs associated with material sourcing and waste processing can be reduced or eliminated. Moreover, demountable structures can be modified, expanded, or repurposed in response to changing needs or functions, thereby enhancing their investment value over time. Notwithstanding these potential benefits, research addressing demountable and reusable STC structures has not been reported in the literature as far as the authors of this contribution are aware.

The disassembly potential of STC beams largely depends on the type of shear connections used to attach the elements and achieve composite action. Mechanical connectors such as screws and bolts are considered the best alternative for this purpose, as their removal is typically a non-destructive procedure. In contrast, glued connections (e.g. plates or other mechanical connectors embedded in glue, or application of glue at the steel-timber interface) or mechanical connectors embedded in grout pockets might require destructive procedures. These methods could cause significant damage to the structural components and require more effort to fully disassemble the components.

Connections with bolts and screws facilitate easy disassembly, however, the reuse of disassembled timber components may be compromised by damage caused by the connectors. For instance, the drilling-unscrewing effects of screws can compromise the integrity and capacity of the connection post-disassembly, and in bolted connections, preloading the bolts leads to premature crushing of timber in the radial direction, hence, full preloading of the bolts cannot be reached. Although there is research on steel-to-timber connections for STC flooring systems, as described earlier in this section, little has been done to tackle these challenges. In response to this, the authors developed and tested three types of bolted shear connections that enable demountability and reusability of STC beam and flooring systems [21,75].

The newly developed shear connections have been tested through push-out tests to assess their load-deformation behaviour and capacity. However, to fully realize their application in STC beams, it is crucial to investigate their behaviour in actual STC beams and their performance under full-scale bending conditions. Therefore, this contribution explores, for the first time, the experimental investigation of two simply supported STC beams with the novel demountable connectors, subjected to six-point bending, both with a span of 10 m and a slab width of 2.51 m. Two types of shear connections that enable demountability and reuse, SCT-1 and SCT-3 have been implemented in these full-scale STC beams, with each beam featuring one type of connection. The tested STC beams consist of a downstanding I-shaped hot-rolled steel profile (IPE 400) and LVL slabs with a thickness of 144 mm connected to the steel profile by means of the novel shear connections. This contribution, details the proposed demountable and reusable STC flooring system, describes the connections used in the STC beams under test, outlines the testing methodology, and presents the results along with their corresponding discussions.

2. Shear connections for demountable steel-timber composite beams and flooring systems

2.1. General

The three steel-to-timber shear connections developed by the authors have been denominated as: shear connection -type 1 (SCT-1), -type 2 (SCT-2), and -type 3 (SCT-3) [21,75]. These novel connections enable disassembly and implement "shear connection devices" that were designed to allow the attainment of the required bolt preload while protecting the timber from crushing exerted by the preload of the bolt, and from damage during serviceability conditions. In the STC beams tested in this contribution, SCT-1 and SCT-3 (see Fig. 1) were implemented in the two full-scale beam specimens, each specimen implementing one type of shear connection.

2.2. Shear connection devices

The shear connection devices shown in Fig. 1, consist of a steel tube made of grade S460 in compliance with EN 10025 [26]. The tube has an outer diameter of 35 mm and a wall thickness of 6.3 mm, with its base welded to a reinforcing steel element, which varies depending on the connection type:

i. for SCT-1, it is a round steel plate (S460 according to EN 10025 [76]) with an outer diameter of 75 mm, a thickness of 10 mm, and an inner hole with a diameter of 22 mm;
ii. for SCT-3, it consists of a rectangular steel plate (S460 according to EN 10025 [76]) 160 × 75 × 15 mm with custom drills to allow the installation of universal partial-thread timber screws ⌀8 × 140 mm (Würth ASSY 4 CSMP, ETA-11/0190 [77]) with an inclination of 60° with respect to the horizontal.

The shear connection devices aim to enhance the connections' performance by:

i. Maximizing embedment in timber due to a substantial contact surface area, especially at the steel-timber interface where significant forces are transferred from the connection device to the timber.
ii. Ensuring slip resistance through the preload of the bolts, allowing for the attainment of adequate preload levels.

It is crucial to note that drilling in the timber must be performed with

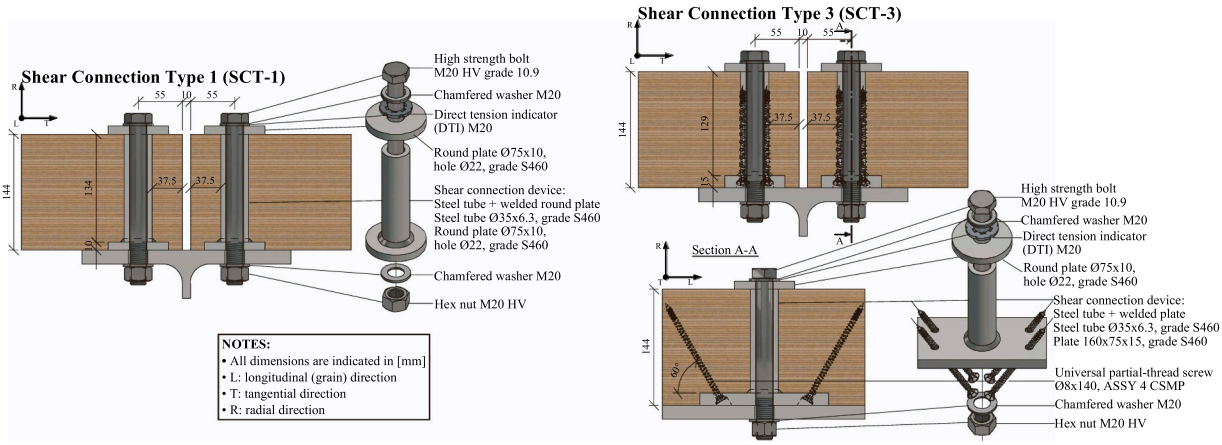

Fig. 1. Details of the shear connections SCT-1 and SCT-3 implemented in the demountable steel-timber composite beams tested in this experimental investigation [21,75].

precision machinery to ensure that the shear connection devices fit perfectly, leaving no clearance between the connection devices and the timber. For the beam tests conducted in this research, the drilling and cutting of the panels were executed using a Hundegger Robot-Drive machine.

2.3. Removable components

In addition to the shear connection device embedded in the timber slab, each connection includes removable components such as bolts, nuts, and washers. The removable components of SCT-1 and SCT-3 are common for both connection types, these components are as follows:

i. A partially threaded high-strength HV bolt M20 × 210 mm grade 10.9
ii. A direct tension indicator (DTI) situated beneath the washer at the bolt head's face
iii. Two washers for HV bolts—one at the bolt head side and another at the nut side
iv. A nut for HV assemblies
v. A round steel plate with the same dimensions as the one welded to the tube's bottom side

Components (i) to (iv) adhere to EN 14399 [78] standards for high-strength HV assemblies. The selection of HV bolts grade 10.9 is deliberate to prevent premature bolt failure due to bearing and shear. The bolt shall be preloaded to 70 % of its ultimate load in accordance with EN 1993–1-8 [79] and EN 1090–2 [80].

2.4. Mechanical performance

The mean load-slip curves obtained in the push-out tests [21,75] for SCT-1 and SCT-3 are presented in Fig. 2. The tests results showed that a friction mechanism (i.e. slip resistance) was activated due to the preload of the bolt. The connections exhibited large deformation capacities that exceeded 40 mm of slip, and in both connections, one plastic hinge developed at the steel-timber interface. In SCT-1, fracture of the bolts was observed, their fracture initiated at a slip of ~70 mm. In SCT-3, the bolts did not fracture, and the tests concluded upon reaching the test setup's maximum available deformation of ~140 mm.

For connectors SCT-1 and SCT-3, the average maximum loads reached were 161.4 kN and 163.8 kN per shear connector, respectively. At 15 mm of slip, the average loads per shear connector were 124.9 kN for SCT-1 and 149.1 kN for SCT-3. To avoid damages in the connectors and in the timber, it is expected that the connectors work at slip values smaller than 6 mm. In the push-out tests, the loads reached at 6 mm were 95.7 kN for SCT-1 and 120.2 kN for SCT-3.

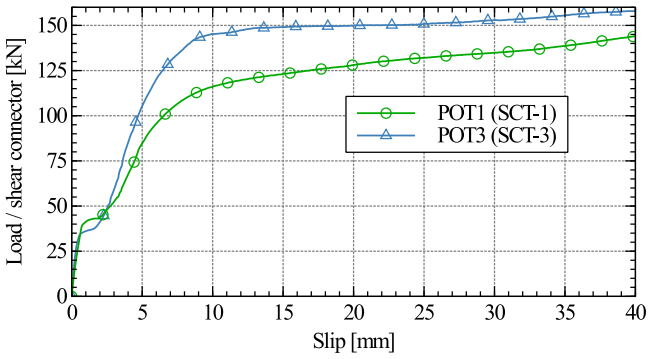

Fig. 2. Mean load-slip curves of SCT-1 and SCT-3 [21,75].

3. Demountable flooring system

In the pursuit of transitioning towards more sustainable practices in the construction sector, one key strategy is the implementation of circular economy and design for disassembly (DfD) principles. These approaches provide environmental and economic benefits as highlighted in the Introduction (Section 1). However, the construction sector faces specific challenges in this transition as traditional construction practices are not well suited for easy disassembly and reuse of structural components. In response to this need for sustainable solutions, a demountable and reusable STC flooring system, comprising downstanding steel beams and LVL slabs, has been developed and tested. Fig. 3 shows the general concept of the demountable and reusable flooring system subject of this investigation.

The development of this flooring system was preceded by the project "Reuse and Demountability Using Steel Structures and the Circular Economy" (REDUCE) project [81], funded by the Research Fund for Coal and Steel (RFCS) under the grant No. 710040. In REDUCE, SCC demountable and reusable flooring systems and shear connections were developed and tested. Additionally, a demonstration building incorporating the concepts developed in REDUCE was built [82,83]. The outcomes of this project laid the foundation for the development of the flooring system discussed in this investigation, wherein concrete slabs were substituted with timber slabs, and novel shear connections were implemented.

The demountable and reusable STC flooring system consists of downstanding I-shaped hot rolled steel profiles with LVL panels on top, connected using novel shear connections that enable demountability

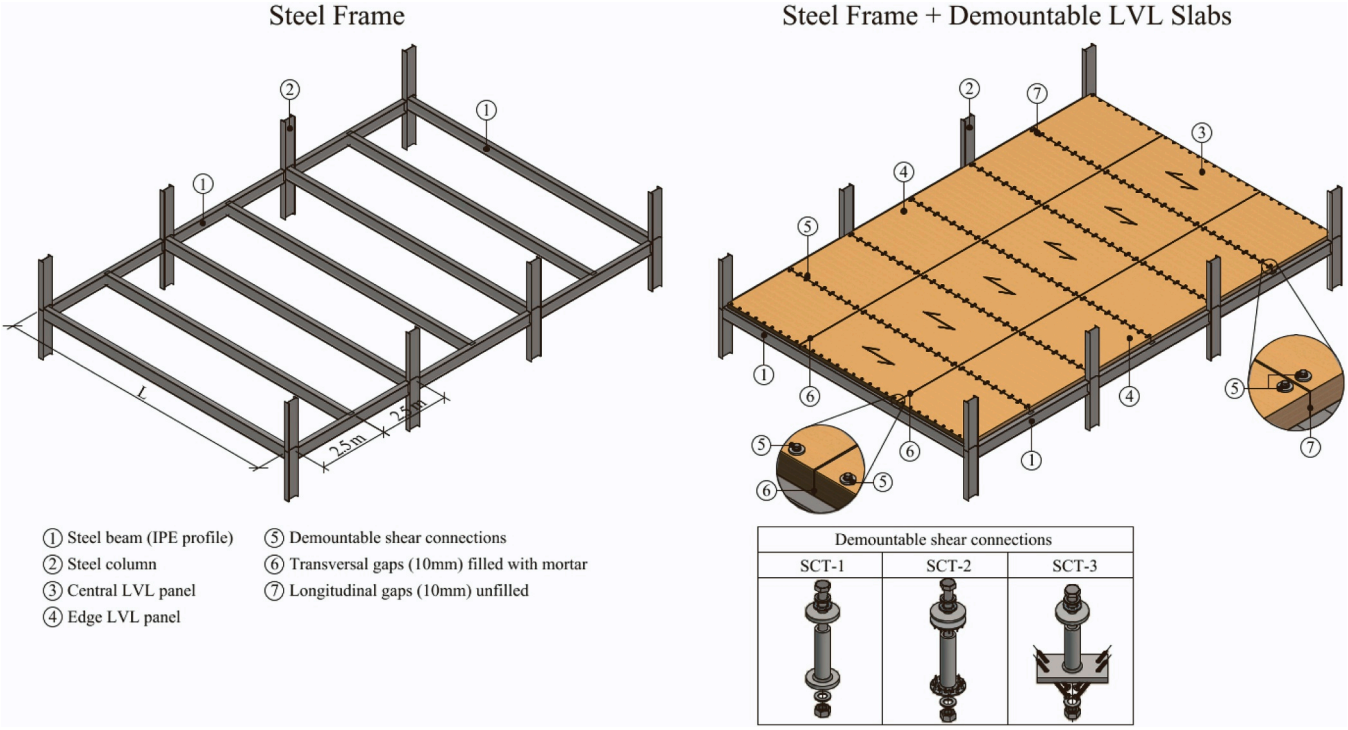

Fig. 3. Demountable STC flooring system concept and novel shear connections that enable demountability and reuse [21,75].

and reuse. LVL has been chosen due to its low variability in mechanical properties and enhanced mechanical performance, which lead to higher mean and characteristic strength values, and to smaller partial safety factors. In this system, the grain direction of the panels was aligned with the longitudinal direction of the beams to obtain the maximum possible strength and stiffness of the STC beams as the main target are long spans for large open spaces.

Crossband LVL (LVL-C, Kerto-Q [84]), which has approximately 20 % of cross veneers, was selected for its superior strength and stiffness in the tangential direction, which are crucial for minimizing deflections in slabs between steel beams. Moreover, as the connections have been placed close to the edge of the panels, the cross veneers provide reinforcement to prevent splitting failure which is likely to occur in products with thicker layers or with the grain of all layers aligned to the load direction such as glulam and CLT [12,13,15,85].

In this experimental study, the LVL-C panels used in the STC beams had a thickness of 144 mm, its layup consists of 48 veneers with a thickness of ~3 mm (see Fig. 4) as follows: II-IIIII-III-III-IIIII-II-IIIII-III-III-IIIII-II, where "I" represents the longitudinal veneers with their grain aligned in the longitudinal direction, and "-" represents the cross veneers with their grain perpendicular to the grain of the "I" veneers.

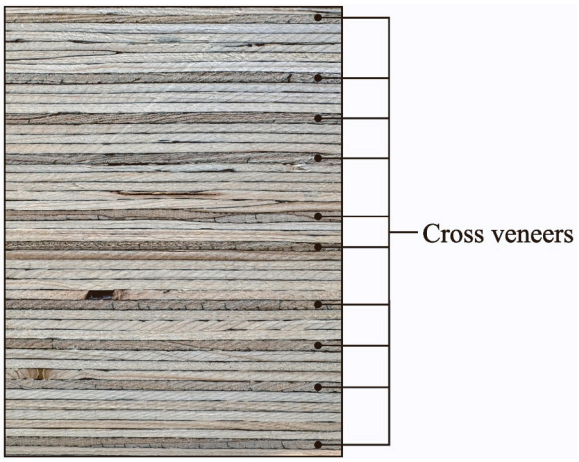

Fig. 4. Layup of the LVL-C used in this investigation.

LVL panels are subject to size limitations, their maximum width (measured in the tangential direction) is capped at 2.5 m, while maximum lengths can vary between 18 and 25 m [86]. Consequently, the panels' width has been set at 2.5 m to optimize the spacing between steel beams. The length of the panels in the longitudinal direction isn't fixed, as it depends on the span requirements. However, when determining their length, factors such as transportation logistics, installation and construction tolerances need to be considered. One approach is to divide the panels along the span into three portions (i.e., edge panels and a central panel), as depicted in Fig. 3. This provides tolerances and facilitates transport and installation, which can be critical for long spans.

A 10 mm gap between adjacent panels, necessary for construction and disassembly tolerances is present. The transversal gaps (perpendicular to the grain direction) are to be filled with mortar to enable compression transfer and to activate the shear connectors in the edge panels. In REDUCE project [81], both SCC demountable slabs without longitudinal gap (i.e. continuous slabs) and those with longitudinal gap were investigated. It was concluded that leaving the gaps unfilled is necessary to facilitate disassembly. In this testing campaign, the longitudinal gaps of the tested STC beams remained unfilled, as filling them does not serve any mechanical function within the system and may complicate the disassembly process.

Prior to pouring the mortar in the transversal gaps, the timber in the gap shall be protected to prevent moisture and bonding between mortar and the LVL panels, it can be protected for instance with a plastic film as done in this testing campaign. This approach also facilitates disassembly, as the mortar, confined within the plastic film, does not bond to the timber elements. Consequently, removal of the mortar and the slab elements is straightforward when they are loose.

This flooring system shows great promise for modularization, standardization, and off-site serial production, making it ideal for prefabrication in standard sizes and modules. This approach could significantly

impact construction time and labor efficiency.

4. Experimental testing campaign

4.1. General

The flexural response of the STC beams was investigated through experimental six-point bending tests on full-scale specimens in simply supported conditions. Two full-scale STC beams were tested: beam test 1 (BT-1) and beam test 2 (BT-2), both specimens consisted of a downstanding I-shaped hot-rolled steel profile with LVL panels on top, connected using shear connectors that enable demountability and reuse. The two STC beam specimens were identical in terms of geometry, materials, and shear connections' arrangement. The difference was the type of shear connection used, BT-1 implemented SCT-1, and BT-2 implemented SCT-3. The two specimens had a total length of 10.6 m, a span of 10 m, and an overall slab width of 2.51 m (see Fig. 5). The tests were conducted at room temperature and under relative humidity conditions, both parameters were monitored with a sensor ALMEMO (FHAD 46-C41), the mean values were 22 °C and 41.1 %, respectively. The moisture content of the LVL slabs was measured using a capacitive moisture sensor ALMEMO (FHA 696 MF), the mean value was 12.9 %.

4.2. Specimen details

The dimensions and details of the specimens are depicted in Fig. 5 and Fig. 6. The two STC beam specimens of this testing campaign consist of a downstanding steel profile IPE400 S355 in accordance with EN 10025 [76] with a length of 10.6 m (Fig. 6.3), and six crossband LVL (LVL-C, Kerto-Q [84]) panels with a thickness of 144 mm, the two central panels (Fig. 6.2) have dimensions 4040 × 1250 × 144 mm, and the four edge panels (Fig. 6.1) have dimensions 3270 × 1250 × 144 mm. The panels were placed on top of the steel beam and connected with the novel shear connectors introduced in Section 2.

Stiffeners (Fig. 6.11) were welded to the steel beam at the points where the load was applied, and at the two supports, stiffeners and extensions of the base to the two sides of the beam (Fig. 6.4) were welded to the steel beam to provide stability. The holes drilled in the flanges of the steel beams had a diameter of 24 mm, allowing for up to 4 mm of clearance for the M20 bolts used in the connection.

Between adjacent panels there was a gap of 10 mm, the transversal gaps (Fig. 6.9) were filled with high strength mortar (PAGEL V1/30 HF [87]) to transfer compression forces and activate the connectors of the edge panels. A plastic film was used to avoid moisture in the LVL panels due to the mortar pouring and prevent bonding between mortar and timber. The longitudinal gap remained unfilled, however, one steel plate (200 ×150 ×10 mm) was placed at the longitudinal gap in each end of the beam (Fig. 6.5) to prevent its closure during the test at large deformations.

Steel plates (400 ×120 ×10 mm) were used to ensure the horizontal alignment of adjacent panels at the transversal gaps, four plates were screwed near the edges of the slabs (Fig. 6.7). It is important to note that these plates are only necessary for testing purposes. In the actual flooring system, the LVL slabs will rest directly on the steel beams, ensuring automatic horizontal alignment without the need for these plates.

Two rows of shear connectors, spaced 120 mm transversally and 337.5 mm longitudinally, were installed in the specimens (Fig. 6.6). The SCT-1 connectors were implemented in BT-1, while SCT-3 connectors were implemented in BT-2. Both types of connections implemented bolts M20 grade 10.9. In accordance with Eurocode 3 [79] and EN 1090–2 [80], these bolts were preloaded to 70 % of their ultimate strength.

The required preload for the bolts M20 grade 10.9 used in this study's connection assemblies was 172 kN. To ensure this minimum preload was reached, one DTI was placed under the washer adjacent to the bolt head. A consistent preload was achieved through a defined tightening procedure, established after testing eight SCT-1 connection assemblies instrumented with a load cell, following a testing approach outlined in [75]. The tightening procedure involved: (i) initially applying a torque of 400 N·m to the bolt head using a torque wrench while holding the nut to prevent its rotation with another wrench, followed by (ii) a 180-degree rotation of the bolt head using a pneumatic wrench. This approach, involving bolt head rotation, was preferred over the typical nut rotation for ease and practicality as working under the slab to tighten the nut is more difficult and requires more effort.

Braces were fixed to the steel beam (Fig. 6.4) to support the panels and prevent stresses on the connections and panels due to the cantilever effect caused by the panels' free edges. These braces were not connected to the panels, ensuring they did not contribute to stiffness and strength. To minimize friction between the steel supports and timber panels, 3 mm thick PTFE plates were used. It is important to note that these braces are only necessary for testing purposes and will not be included in the actual flooring system.

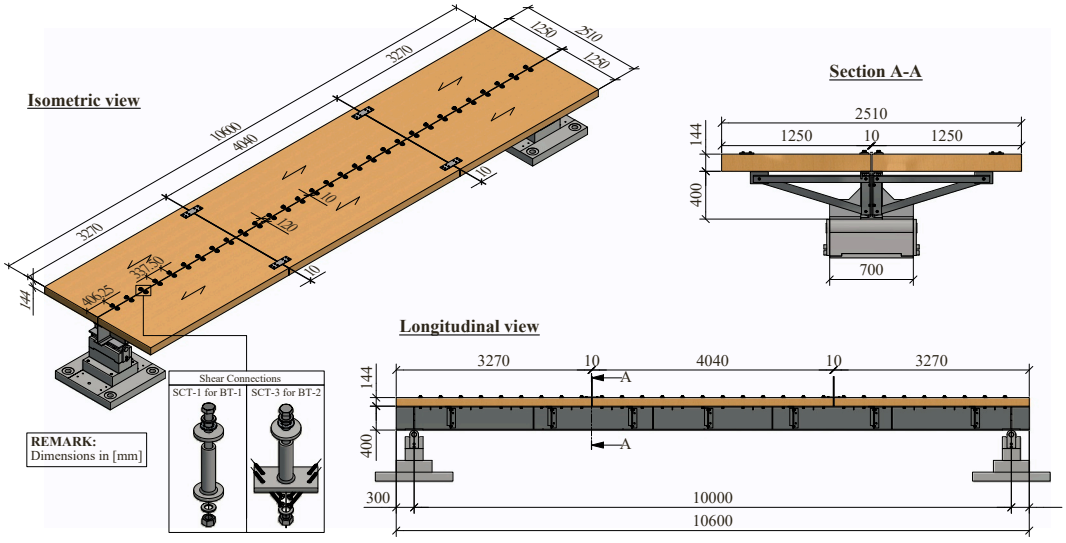

Fig. 5. Dimensions of the tested specimens.

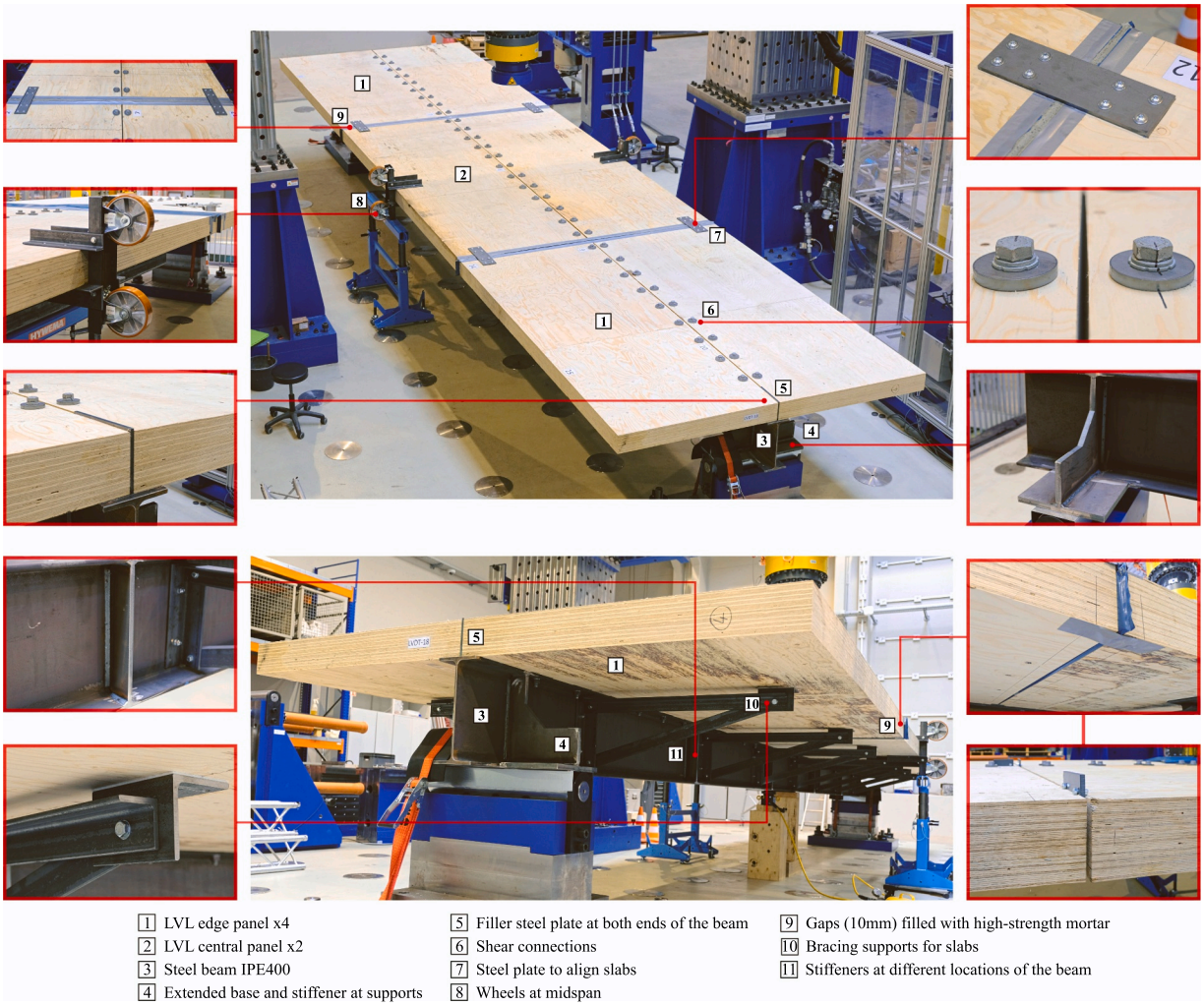

Fig. 6. Components of the STC beam specimens.

4.3. Assembly process

The assembly process of the STC beam specimens is crucial for understanding the actual flooring system's assembly and identifying potential improvements in efficiency, cost, and execution time. Preliminary works on the components must be conducted offsite to minimize on-site execution times and errors, thereby ensuring the highest possible quality. This means all elements must be prepared offsite to be ready for installation, facilitating their subsequent connection to other components onsite. This subsection describes the preliminary works and the assembly process of the two specimens, which was the same for both, the specimen of BT-1 and the specimen of BT-2.

Prior to the assembly, the steel beams' drillings for the bolts were done, and the stiffeners and the extended bases at the supports were welded in a dedicated area for this purpose in the laboratory hall. The cutting and drilling works of the panels were executed in a specialized workshop, the connection devices were also installed in the timber panels before starting the assembly of the specimens, pictures of these processes are shown in Fig. 7.

The assembly process was the same for the two STC beam specimens, pictures of the process are shown in Fig. 8. First the steel beam (IPE 400) was transported to the strong floor of the laboratory hall and placed at the two supports (Fig. 8.1). Ratchet straps were used to secure the specimen at the supports during the assembly process. These straps were removed when the assembly was completed, and just before the tests started. The supporting braces were connected to the web of the beam using bolts and the supporting surface's arm was aligned with the surface of the top flange of the beam (Fig. 8.2 and Fig. 8.3). After that, LVL panels were placed one by one on top of the steel beam, at this stage the bolts were placed but not yet tightened (Fig. 8.4 and Fig. 8.5). Once all the timber plates were in its final position, and the bolts had been placed, the tightening of the bolts was done as described in Section 4.2. Additionally, wheels were installed at midspan (see Fig. 6.8) to guide the specimen vertically during the test. The movement of these wheels was confined using a channel steel section fixed with rods to the portal frame as shown in the test setup Section 4.5 (see Fig. 10.6). Then, the timber was protected with a plastic film at the gaps and the mortar was poured (Fig. 8.7), manual tools were used to pour the mortar, to consolidate it in the gap, and to remove air pockets and ensure that the mortar was evenly distributed and void-free. This mortar reaches a compressive strength of at least 70 MPa in 24 h according to the technical specifications of the supplier [87]. Immediately after pouring the mortar in the gaps, steel plates were installed at the gaps and near the edges of the panels to achieve horizontal alignment of the timber slabs (Fig. 8.8).

4.4. Mechanical properties of structural steel and LVL

4.4.1. Structural steel

Tensile tests were conducted according to EN ISO 6892–1 [88] in order to determine the mechanical properties of the structural steel S355 of the steel beams. Four coupon shape specimens were taken from each

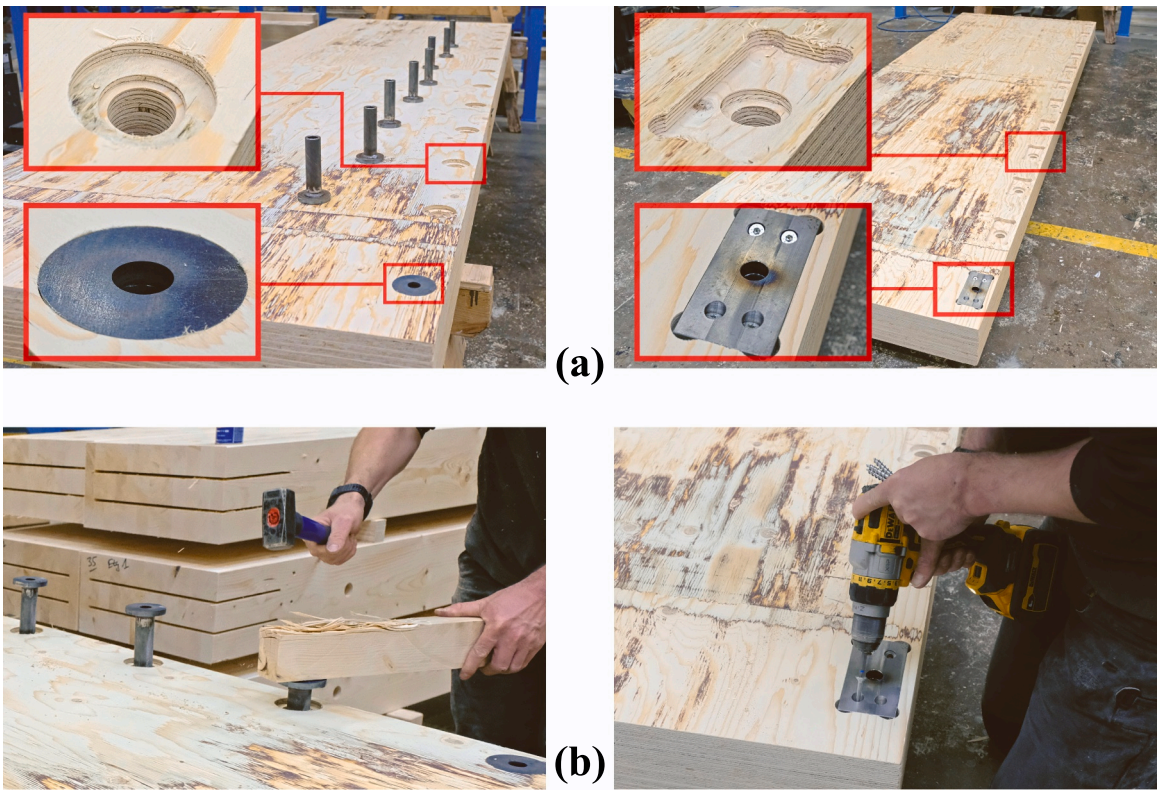

Fig. 7. Pictures of the preliminary woodworks: (a) drill details of the two types of connection SCT-1 and SCT-3, and (b) installation of the shear connection devices of the two types of shear connection.

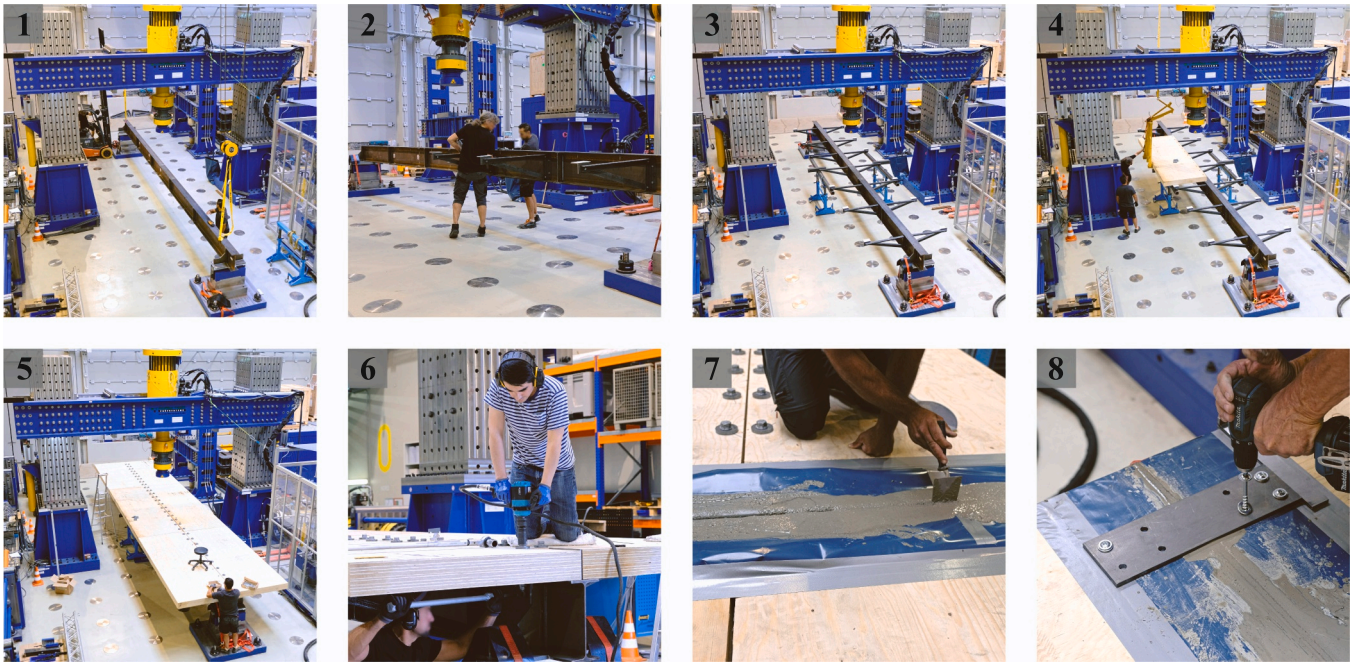

Fig. 8. Pictures of the assembly process.

of the two steel beams IPE 400 S355 of the specimens BT-1 and BT-2. A mean yield strength of 399 MPa with a coefficient of variation (CV) of 1.7 %, a mean ultimate strength of 512 MPa with a CV of 1.7 %, and a mean modulus of elasticity of 207 GPa with a CV of 1.9 %, were obtained.

4.4.2. *Laminated veneer lumber (LVL)*

The LVL slabs were made of crossband LVL crafted from spruce wood (Kerto-Q [84]). A comprehensive testing campaign was conducted to determine strength and stiffness properties of this engineered timber product in the three main orthogonal directions (see Fig. 9) under compression, tension, shear, and bending conditions. The testing

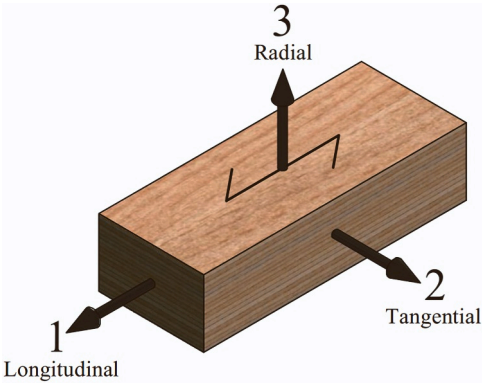

Fig. 9. LVL material directions.

procedures and the results of the testing campaign have been reported in [89], a summary of key properties is presented in Table 1.

4.5. Test setup and instrumentation

The test setup and the instrumentation of the steel beams is depicted in Fig. 10. The instrumentation layout is illustrated in Fig. 11. The tests were carried out at the Laboratory of Engineering Structures of the University of Luxembourg in a Test portal PP 4000 HK-2DH (Form+Test) equipped with a hydraulic jack to apply the load vertically, it has a capacity of 4 MN. The beams were simply supported at two points and the load was transferred to the beam with spreader beams that apply the load at four points through rollers with a length of 800 mm. These rollers rest on a set of plates (see Fig. 10.7), from top (next to the rollers) to bottom (next to the LVL slabs), as follows: a steel plate (800 ×200 ×10 mm), a PTFE plate (800 ×200 ×3 mm), a steel plate (800 ×200 ×10 mm), and a neoprene strip (800 ×200 ×5 mm).

The instrumentation of the STC beam consisted of strain gauges (DMS) installed in the steel beam, linear variable differential transformers (LVDTs) and laser sensors that were placed at different locations to monitor relevant displacements. At different sections of the LVL slabs, LVTDs were placed at the top and at the soffit, to monitor local deformations and to later obtain strains. The endslip at both ends of the beam was monitored with LVDTs. Similarly, the slip along the beam was monitored at different locations along the beam with LVTDs installed at the edge of the top flange of the steel beam. LVDTs and laser sensors were placed under the STC beam, on the strong floor to monitor the deflection of the beam at the bottom flange of the steel beam and at different locations along the beam. In addition, the strains in the steel beam were monitored using strain gauges that were installed in three sections of the steel beam at the inner faces of the top and bottom flanges of the beam.

Table 1
Mean strength and elasticity modulus of LVL-C (Kerto-Q) obtained experimentally.

Strength		Modulus of elasticity	
Notation	**Value [MPa]**	**Notation**	**Value [MPa]**
$f_{c,1}$	40.4	$E_{c,1}$	7 917.1
$f_{c,2}$	11.1	$E_{c,2}$	1 764.5
$f_{c,3}$	4.0	$E_{c,3}$	95.5
$f_{t,1}$	37.8	$E_{t,1}$	10 680.0
$f_{t,2}$	8.3	$E_{t,2}$	2 199.9
$f_{t,3}$	0.6	$E_{t,3}$	92.1

Definition of Subindexes: c, compression; t, tension; 1, longitudinal direction; 2, tangential direction; 3, radial direction

4.6. Loading procedure

In these simply supported beams tested in 6-point bending, the load was applied symmetrically at four points on the top surface of the LVL slabs using a spreader beam to transfer the load, the details are shown in Fig. 12. In this testing campaign the 6-point bending test setup was established to impose conditions on the STC beams comparable to that induced by a uniformly distributed load as it is the standard situation for structural analyses. The loading strips at each loading point were 800 mm long in the transversal direction, the distance from the support to the first loading point was 2 m, similarly, the distance between the four loading points was 2 m.

Due to the lack of testing standards targeting specifically STC structures, the loading procedure implemented in this study was based on the loading procedures established in EN 26891 [90] and Eurocode 4, Annex B. The loading procedure presented schematically in Fig. 13, shows that the specimens were initially loaded to around 40 % of the estimated maximum load (P_{est}) and unloaded to 10 % of P_{est} as established in the initial loading-unloading cycle of EN 26891. To assess the response of the STC system in the elastic range (e.g. serviceability conditions), 25 cycles within $0.1P_{est}$ and $0.4P_{est}$ were applied. Then, the specimen was gradually loaded in several incremental steps, the load values corresponding to the different load levels indicated in Fig. 13 are presented in Table 2. In both tests the load was applied at a rate of 0.2 mm/s.

The loading procedure was similar for the two tested STC beams, however, in BT-1 the specimen was unloaded after reaching a load of 674 kN and a midspan deflection of ~400 mm because the maximum travel of the hydraulic jack was reached. In BT-2 this issue was addressed, an extension arm was added to the hydraulic jack to increase the travel range, nevertheless, BT-2 was stopped when the maximum midspan deflection for this test setup was reached (i.e. ~650 mm).

5. Results and discussion

5.1. Load-deflection of the STC beams

Pictures showing the deformed shape of an STC beam at different loading stages are depicted in Fig. 14. The moment-midspan deflection and load-midspan deflection curves obtained from BT-1 and BT-2 are presented in Fig. 15a and Fig. 17a, and the de deflection along the beam, measured with LVDT and laser sensors, for different loading stages is shown in Fig. 15b and Fig. 17b.

In Fig. 15a, Fig. 17a and in Table 2, the moment (M) corresponds to the moment at midspan estimated considering an even distribution of forces at each of the four points where a load of $P/4$ was applied, and the force (P) corresponds to the total force applied to the specimen. Hence, the moment was estimated as $M = 6P{\cdot}\ell/40$.

Both beams exhibited similar response in terms of load-deflection, additionally, the load and the corresponding midspan deflection values at different loading stages are presented in Table 2. The response of the beam changed from linear to nonlinear at a load of about 400 kN (moment of 600 kN·m) and a deflection of ~60 mm, in both tests. This began around loading stage III, closely coinciding with the yielding of the bottom flange in the steel profile at the midspan section (section E), which occurred between loading stages III and IV. The yielding of the bottom flange was identified when the strain exceeded 1.9 ‰. Additionally, when a load of about 600 kN (moment of 900 kN·m) was reached, the load-deflection curve flattened significantly.

In BT-1, the maximum load reached was 674 kN (moment of 1011 kN·m) while BT-2 reached a maximum load of 686 kN (moment of 1029 kN·m). Remarkably, these values are nearly twice the plastic bending resistance of the IPE 400 (i.e. 521 kN·m), which is calculated considering the actual properties of the steel profile, a yielding strength of 399 MPa and a modulus of elasticity of 207 GPa (see Section 4.4.1).

In BT-2, after loading stage VIII, in the subsequent loading phase, a

Fig. 10. Test setup and instrumentation of the STC beams.

sudden drop of the load was observed. This drop was linked to mortar crushing in one of the gaps and delamination of the LVL near this gap. The maximum deformations observed in the two tests were ~400 mm and ~650 mm, respectively for BT-1 and BT-2, which demonstrate the large deformation capacity of the tested STC beams. However, it is crucial to highlight that the termination of both tests was dictated by the maximum deformation capacity of the test setup, rather than the complete fracture of the specimens. Notably, the test BT-1 was stopped at a smaller deflection compared to BT-2, attributed to the latter having an extended range of the jack's travel due to an added arm extension, a modification not implemented in BT-1.

5.2. Slope of the elastic branch in the load-deflection curve

The slope of the elastic branch in the load-deflection curve (k_{el}) values were 6.4 kN/mm for BT-1 and 7.2 kN/mm for BT-2. These values were calculated considering the forces and displacements corresponding to loading stages I and II, which are within the linear branch of the load-deflection curves. In the moment-midspan deflection curves in Fig. 15a and Fig. 17a it is evident that there was no loss of stiffness during the 25 loading-unloading cycles within the elastic range (i.e. service conditions). In the 25th loading cycle, bending stiffness values were recorded at 7.7 kN/mm for BT-1 and 8.0 kN/mm for BT-2.

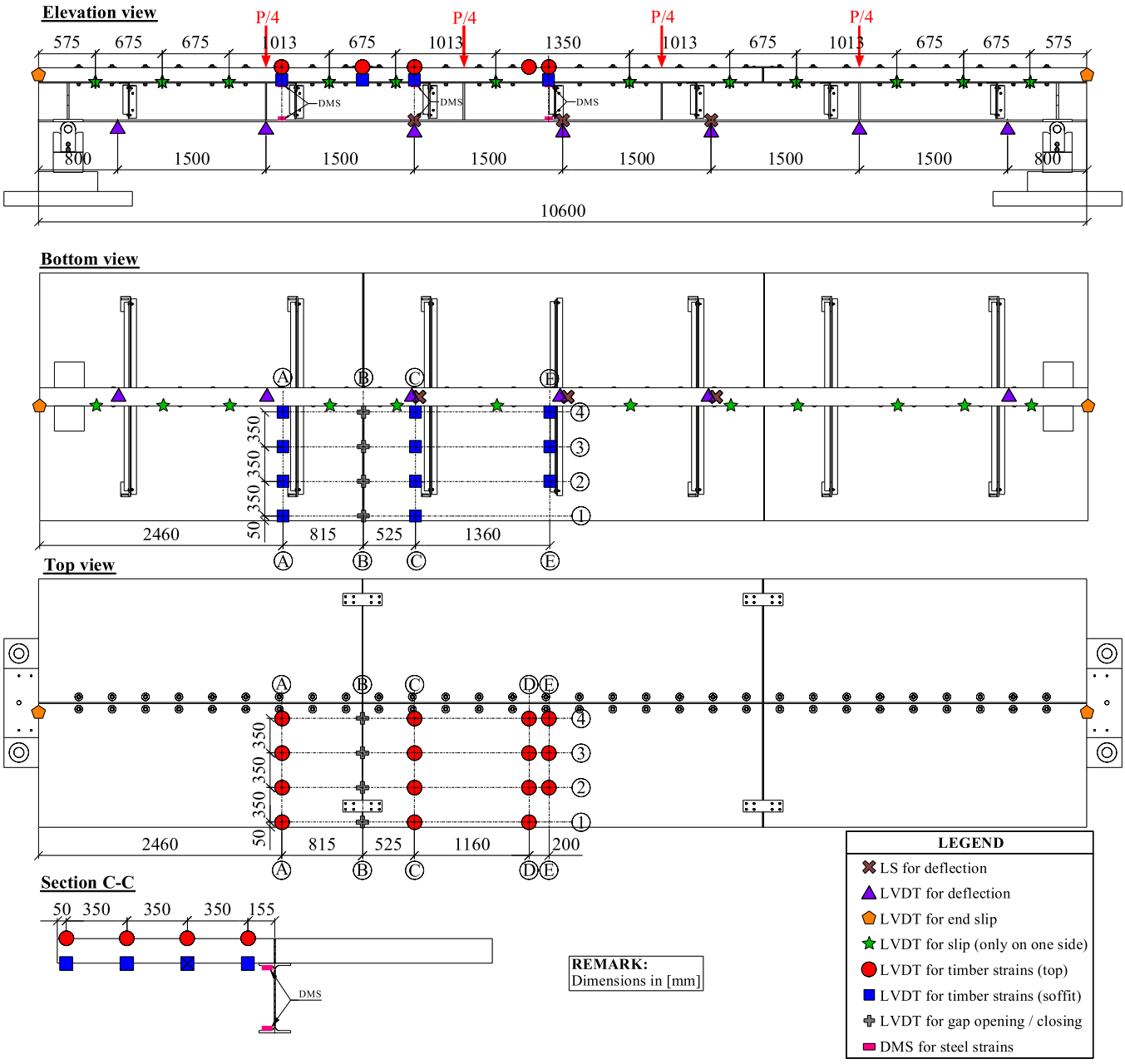

Fig. 11. Instrumentation layout of the STC beams.

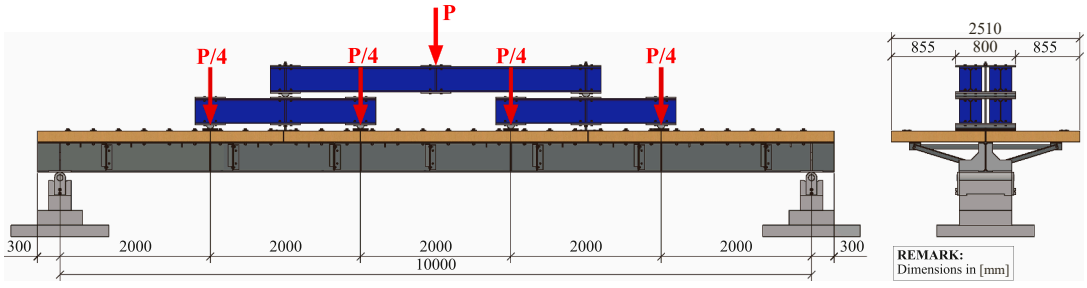

Fig. 12. Details of the load introduction.

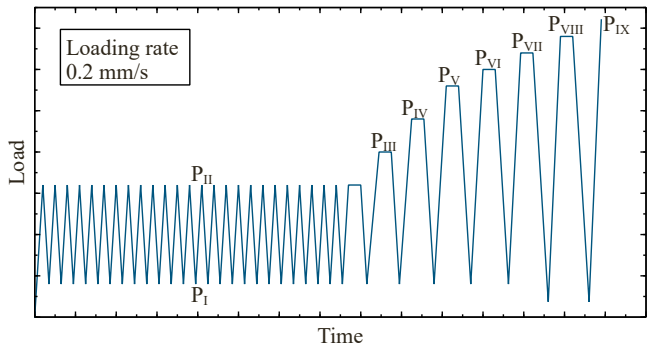

Fig. 13. Schematic representation of the time history of the applied load.

5.3. Slip measurements and shear connectors response

The slip distribution along the beam was recorded with LVDTs placed in one side of the top flange of the steel beam (see Fig. 10 and Fig. 11). The slip distribution for different loading stages is illustrated in Fig. 15c and Fig. 17c for BT-1 and BT-2, respectively. In general, the largest slip values were observed in the last three connectors. However, in BT-1 the largest slip values were observed near the third shear connector at both ends of the beam (see Fig. 15c). Table 2 presents the maximum slip values obtained at different loading stages.

In BT-1 the slip distribution was almost symmetrical with respect to the midspan line with similar slip values in both halves of the beam, whereas in BT-2 the shape of the slip distribution was similar but the slip values were slightly larger in one half of the beam. The observed slip distributions in both beams align with the expected patterns, gradually increasing from the midspan towards the edges, and uninterrupted by the transversal gaps. This indicates that the mortar effectively transferred compression loads from the central to the edge panels, thereby activating the shear connectors of the edge panels.

In BT-1, at loading stage VIII the maximum slip values recorded in each half of the beam were 5.3 mm and 4.8 mm. In BT-2, at a similar load level in loading stage VIII, maximum slip values of 6.3 mm and 4.1 mm were recorded at each half of the beam. The difference of slip values observed in both halves of the beams is related to the alignment of the bolts in the holes of the beam, the half of the beam with smaller slip values indicates that the clearance between the bolts and the flange of the steel beam was smaller. Since the bolts have a diameter of 20 mm and the diameter of the holes is 24 mm the clearance can be any value within the range of 0 to 4 mm.

Within the elastic range (i.e. up to loading stage III) the maximum slip values were smaller than 1 mm in both beams. Since these values are relatively small compared to the deformation capacity of the connections observed in the push out tests [75], this showcases the reuse potential of the timber slabs when the loads acting on the beams remain within the elastic range (i.e. serviceability limit states). Moreover, even at the last loading stage, the most stressed connections remained undamaged, with an observed embedment of approximately 1 mm in the timber, demonstrating the connections' robustness.

Table 2
Parameters obtained at different loading stages.

Test	Loading Stage	Load	Moment	Midspan Deflection	Maximum Slip	Strains*					
						Section A		Section C		Section E	
		P [kN]	M [kN·m]	w [mm]	δ [mm]	ε_{timber} [‰]	ε_{steel} [‰]	ε_{timber} [‰]	ε_{steel} [‰]	ε_{timber} [‰]	ε_{steel} [‰]
BT-1	I	82.6	123.9	12.0	0.4	-0.18 (0.09)	-0.22 (0.26)	-0.12 (−0.07)	-0.32 (0.4)	-0.22 (−0.01)	-0.14 (0.40)
	II	317.9	476.8	48.8	0.6	-0.40 (0.07)	-0.51 (0.95)	-0.59 (−0.25)	-0.62 1.29	-0.71 (−0.09)	-0.30 (1.34)
	III	399.0	598.6	61.5	0.7	-0.43 (0.13)	-0.63 (1.18)	-0.79 (−0.30)	-0.75 (1.62)	-0.97 (−0.10)	-0.31 (1.35)
	IV	478.5	717.7	84.5	1.2	-0.44 (0.25)	-0.87 (1.45)	-1.06 (−0.28)	-0.92 (1.76)	-1.35 (0.00)	-0.48 (3.23)
	V	559.4	839.0	137.4	1.8	-0.36 (0.26)	-1.00 (1.69)	-1.66 (−0.01)	-1.12 (2.28)	-2.16 (0.39)	-0.40 (3.45)
	VI	639.4	959.2	265.8	3.3	-0.12 (0.17)	-1.07 (2.00)	-3.11 (1.64)	-1.13 (2.37)	-3.55 (1.11)	-0.28 (12.32)
	VII	659.9	989.9	330.7	4.4	-0.14 (0.15)	-1.1 (2.20)	-3.78 (2.35)	-1.13 (3.9)	-4.09 (1.50)	-0.33 (16.45)
	VIII	674.0	1011.0	398.0	5.3	-0.35 (0.15)	-1.17 (2.28)	-4.59 (3.06)	-1.39 (14.01)	-4.69 (1.74)	-0.27 (19.07)
BT-2	I	80.5	120.7	11.2	0.1	0.06 (0.00)	-0.10 (0.24)	-0.14 (−0.08)	-0.15 (0.32)	-0.20 (−0.05)	-0.06 (0.32)
	II	317.0	475.5	44.2	0.6	0.11 (0.07)	-0.40 (0.95)	-0.59 (0.02)	-0.46 (1.26)	-0.66 (−0.13)	-0.21 (1.33)
	III	396.2	594.3	59.1	0.8	0.12 (0.24)	-0.51 (1.19)	-0.81 (−0.02)	-0.6 (1.64)	-0.92 (−0.16)	-0.29 (1.81)
	IV	476.1	714.2	82.0	1.4	0.13 (0.37)	-0.69 (1.45)	-1.07 (0.06)	-0.79 (3.25)	-1.27 (−0.08)	-0.34 (2.26)
	V	557.2	835.7	140.5	2.2	0.04 (0.35)	-0.69 (1.73)	-1.65 (0.33)	-1.01 (5.07)	-1.97 (0.33)	-0.28 (3.15)
	VI	636.8	955.3	288.6	3.7	-0.88 (0.22)	-0.42 (2.52)	-3.46 (1.13)	-1.04 (13.34)	-2.99 (1.21)	-0.28 (18.69)
	VII	649.7	974.6	347.7	4.3	-1.20 (0.26)	-0.32 (2.87)	-4.34 (1.43)	-1.11 (19.86)	-3.31 (1.53)	-0.14 (20.23)
	VIII	686.0	1029.0	512.6	6.3	-1.86 (0.46)	-0.20 (3.68)	-11.46 (2.39)	-1.03 (31.02)	-3.99 (2.17)	0.35 (20.40)
	IX	646.6	969.9	653.0	6.6	-1.67 (0.22)	-0.54 (4.06)	-16.12 (1.08)	-2.57 (44.33)	-3.96 (2.11)	0.10 (20.27)

* The strain values inside parenthesis correspond to the strain values in the soffit of the timber or the steel, whereas the values that are not inside parenthesis correspond to the strain values on the top of the section in the timber or in the steel portion of the section.

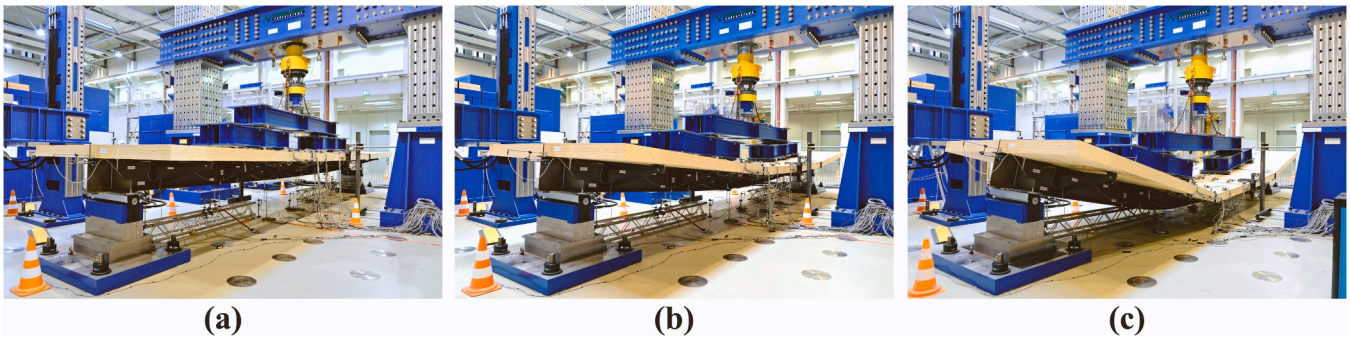

Fig. 14. Pictures taken during the beam test at different loading stages: (a) Loading stage III; (b) loading stage VI; (c) loading stage IX.

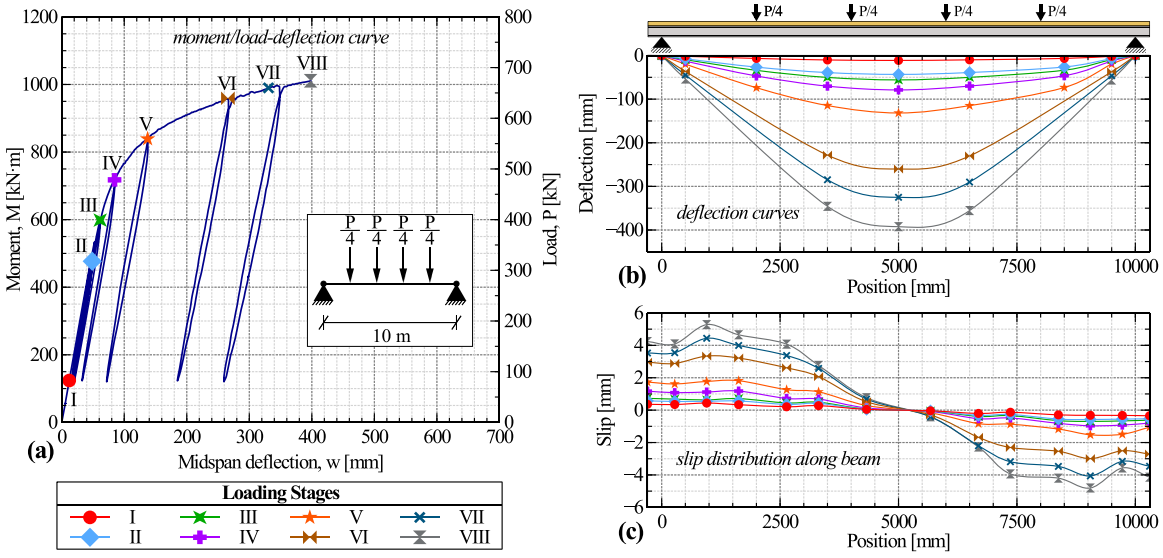

Fig. 15. Load-deformation response of BT-1.

5.4. Strains in the timber slabs and effective width

The strains were measured at sections A, C, D, and E (see Fig. 11) of the slabs in the top and the soffit. The strains recorded in these sections for different loading stages are shown in Fig. 16 and Fig. 18. The largest compression and tension strain values were recorded in the midspan section (section E).

The results show that the strains distribution in the timber along the section is non-uniform. In the sections located in the central slab panel (Sections C, D and E) the strains are larger near the longitudinal axis of the beam and decrease towards the free edge of the panels. This indicates the presence of shear lag effects which are to be considered when analyzing the resistance of the cross-section, because the width of the slab might not be fully utilized. Additionally, in sections C, D, and E negative strains were recorded in the sensors placed on the top surface of the slab indicating compression of the top fibers in the entire width of the timber slab. Analogously, in the sensors installed on the soffit of the slab, positive strain values were recorded, indicating tension of the bottom fibers in the entire width of the timber slab.

Eurocode 5 [41] does not include a definition of the effective width for LVL or CLT in composite sections. For timber cross sections combining LVL ribs and LVL panels, it is common practice to define the effective width as one tenth of the span length ($\ell/10$) [86] as indicated in Eurocode 5 for plywood. Nevertheless, background supporting this assumption is lacking. Further to this, as mentioned earlier in Section 1, little is mentioned in the literature concerning the definition of an effective width for STC beams. There are studies on the effective width of CLT slabs connected to timber beams, for instance Masoudnia et al. [91] proposed a formulation that depends on several parameters such as the thickness of the layers, the span, and the modulus of elasticity. Similarly, Kleinhenz et al. [92] found that the effective width of timber composite beams with CLT panels and glulam ribs is on average 0.15ℓ or $\ell/6.67$. Concerning, composite cross sections with LVL panels as slabs, nothing has been reported in the literature as far as the authors of this contribution are aware.

Considering the measurements of strains at midspan in section E, an effective width was estimated according to Eq. 1, where $\int \varepsilon_{xx} dy$ is the integral of the strain distribution measured at the top of the timber slab, and $\varepsilon_{xx,\max}$ is the maximum absolute strain measured at the top of the timber slab.

$$b_{eff} = \frac{\int \varepsilon_{xx} dy}{\varepsilon_{xx,\max}} \tag{1}$$

Strain measurements were taken only across half of the timber slab's width and at a limited number of points, leaving the strain values at certain locations (e.g., the edge, the center, the other half of the slab) unknown. The measured values were extrapolated, a symmetric distribution was assumed, and the links between measured points were treated as straight lines for calculation purposes. Fig. 19 shows the strain distributions considered for BT-1 at section E. Based on the strains measured during the final loading stage, effective widths of 1881 mm for BT-1 and 1771 mm for BT-2 were determined, corresponding to an effective width of approximately $\ell/5.5$.

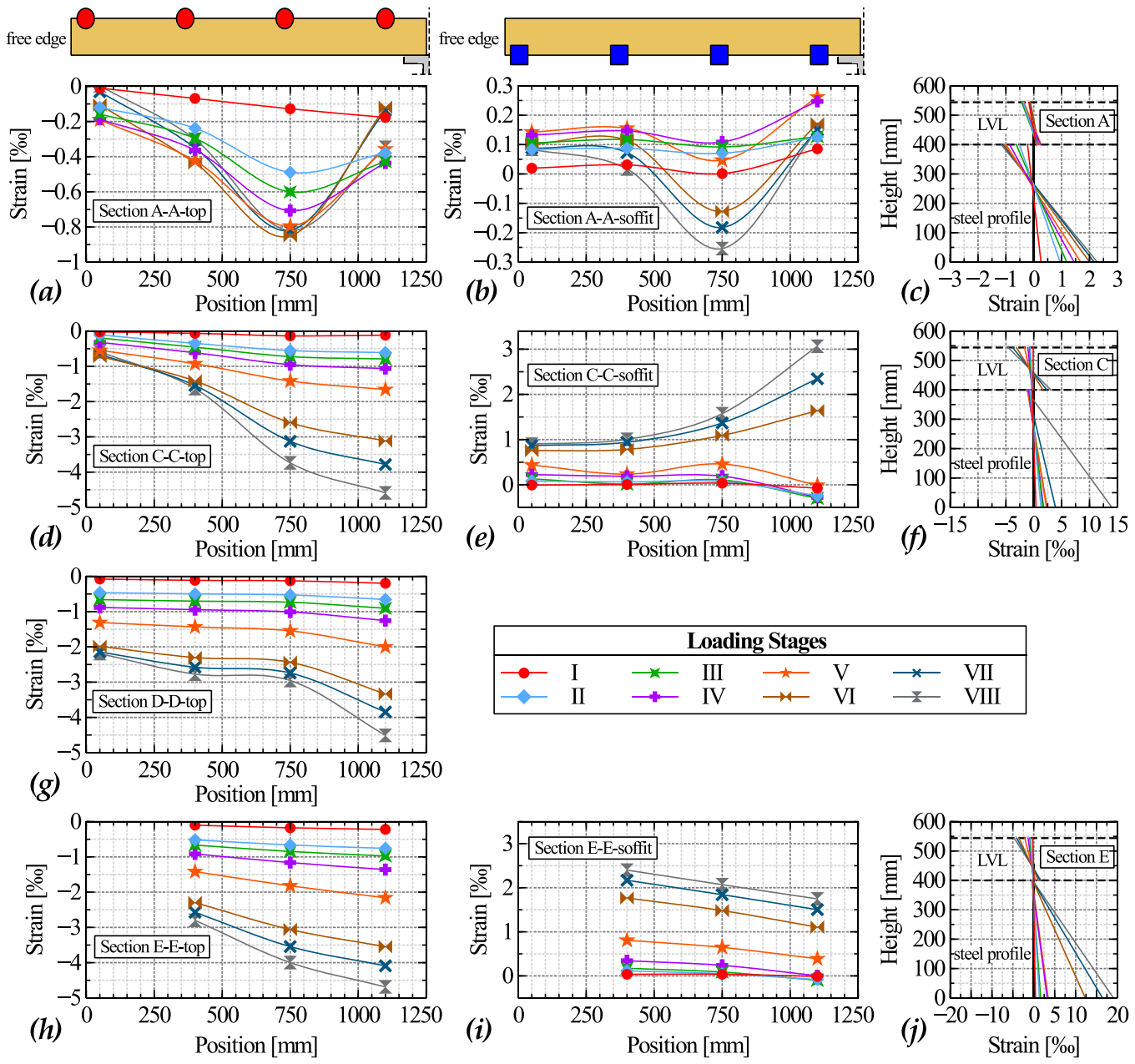

Fig. 16. Strains in the timber slab and strain distributions through the depth of different sections of BT-1.

5.5. *Strain distribution through the depth of the STC beam*

The strain distribution through the depth of the STC beam is shown in Fig. 16 and Fig. 18, in subfigures (c), (f) and (j) respectively for sections A, C and E. These plots were built considering the measurements of the sensors located at Section 4 (see Fig. 11) for the strains in the LVL slab, and the measurements of the DMS sensors installed in the steel section. The values for different loading stages are presented in Table 2. The results show that most of the steel section was in tension during the test whereas the timber was almost in full compression in the initial loading stages and then as the deflection and curvature increased the timber started to take tension at the soffit and the compression increased at the top.

Experimental results of the LVL showed that the proportional limit of the timber is reached at a strain of about 5 ‰, whereas the strain corresponding to the proportional limit of the steel S355 obtained experimentally is 1.9 ‰. According to this, the timber remained within the elastic range throughout the test and the steel beam surpassed its proportional limit at the bottom flange located in the midspan section at loading stage III. This is consistent with the transition from linear to nonlinear behaviour observed in the moment-midspan deflection curves.

In the BT-2 there was a redistribution of stresses which developed from loading stage VI onwards. From this loading stage the strains in the bottom flange of the steel beam increased significantly in subsequent loading stages at section C, from 13.3 ‰ in loading stage VI to 44.3 ‰ in loading stage IX, whereas in the midspan in section E, the strains increased from 18.7 ‰ in loading stage VI to 20.3 ‰ in loading stage IX. In fact, the strain distribution lines for the steel section, as shown in Fig. 18j and Table 2 for loading stages VII, VIII, and IX, overlap, indicating that there is no significant increase in stress within the steel profile at the midspan section. This suggests that there was a redistribution of stresses in which the regions near the transversal gaps filled with mortar became the most stressed regions of the beam.

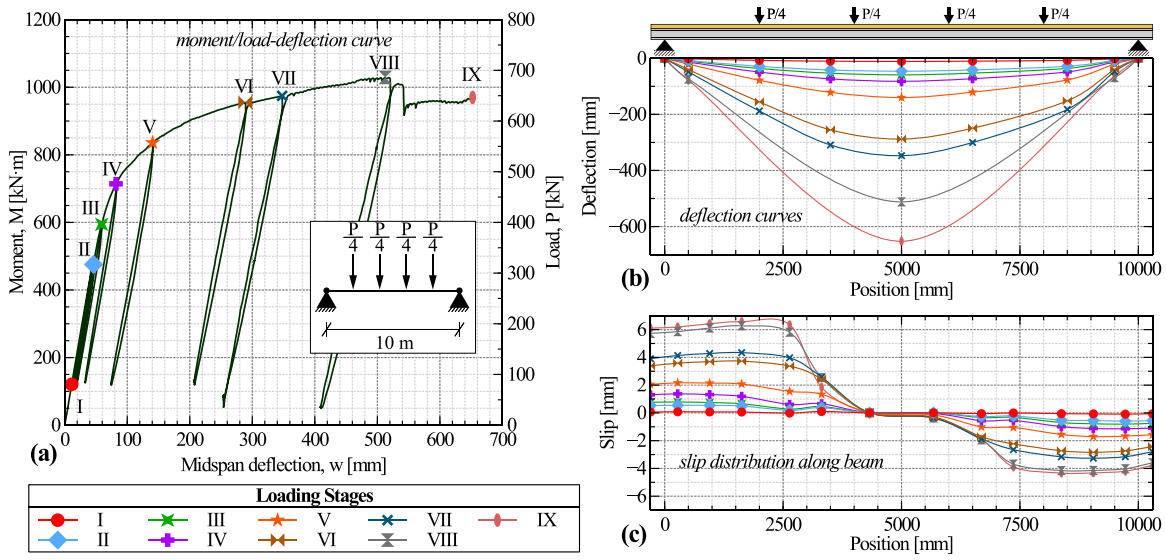

Fig. 17. Load-deformation response of BT-2.

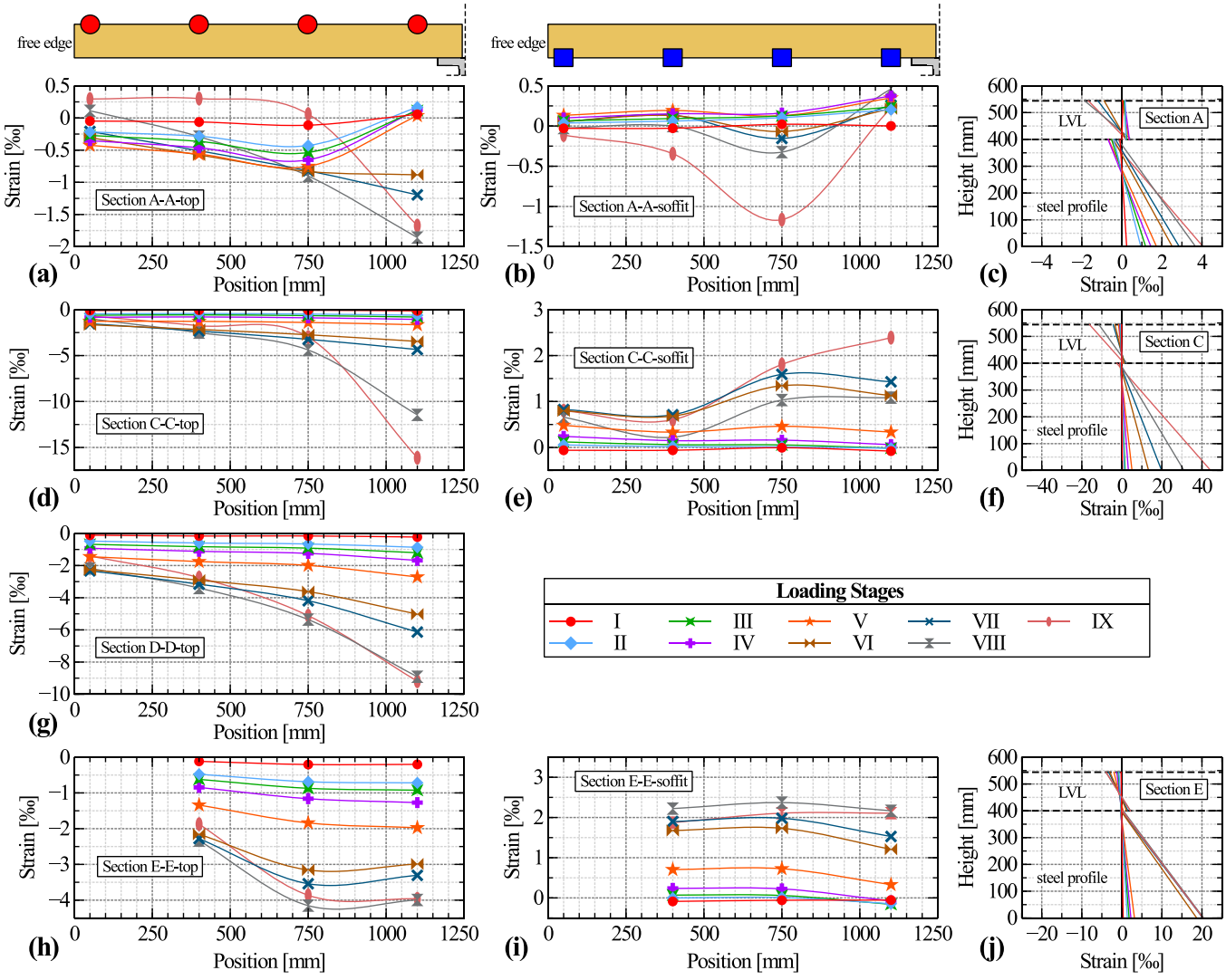

Fig. 18. Strains in the timber slab and strain distributions through the depth of different sections of BT-2.

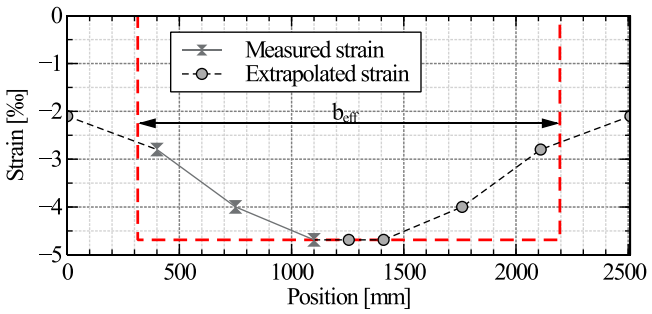

Fig. 19. Strain distribution at section E of the STC beam of BT-1 and effective width.

According to these observations, at the ultimate limit state, the timber slab is capable of withstanding significant loads while remaining within the elastic range. In contrast, the steel beam may enter into plasticity, thereby enabling the use of its plastic capacity. Additionally, when analyzing the bending capacity of this STC beam, three critical sections must be considered: the midspan section and the two sections at the joints where the gaps are filled with mortar.

5.6. Gap opening measurements

LVDT sensors were positioned at section B-B (see Fig. 11) at the gap's location to monitor the opening of the gap as the load increased. The measurements obtained at various loading stages are depicted in Fig. 19. In the graphs, the horizontal axis represents half of the slab's width where the sensors were positioned; with position 0 mm at the slab's free edge and position 1250 mm at the center of the slab width.

For both beams, the gap openings were smaller near the center of the slab, proximate to the slab-to-beam connection, and gradually expanded towards the free edge, where larger displacements were observed. Up to loading stage V, the gap opening in both beams remained under 4 mm. Beyond this stage, the gap opening increased significantly. In BT-1, by the last loading stage (i.e. VIII), the gap opening was approximately 3 mm near the connection and approximately 13 mm near the free edge. In BT-2, at the final loading stage (i.e. IX), the gap opening was around 8 mm near the connection and approximately 34 mm towards the free edge.

5.7. Failure mode

In the specimen of BT-1 the steel beam plasticized and exhibited permanent deformations, however, no significant damages or local failures (e.g. buckling, fracture) were observed in the steel profile, and the midspan section exhibited the largest degree of plasticization. Although the deformation was large, the timber remained within the elastic range and there were no damages at the vicinity of the transversal gaps (see Fig. 21 (c) and (e)), and the mortar did not fracture. This demonstrates that even at large deformations, the integrity of the mortar used to fill the gaps can be preserved. Furthermore, the most stressed shear connections remained undamaged, no noticeable damage was observed in the timber and in the holes of the beam flange (see Fig. 20).

In the specimen of BT-2 the steel beam also plasticized, though to a larger degree as it underwent larger deformations. Similar to the specimen of BT-1, no significant damages or local failures were observed in the steel profile. The shear connection and the holes of the steel beam did not show damage (see Fig. 20). In BT-2, there was a redistribution of stresses leading to plasticization of the steel beams in the region near the transversal gaps, in which the recorded strains of the steel beam were larger than the strains in the midspan section in the last two loading stages. Additionally, the deformations and damages in the mortar and the timber close to the gap were larger, and the load drop observed after loading stage VIII was linked to crushing of the mortar in the transversal gap and delamination of the LVL (see Fig. 21d and Fig. 21f). Notwithstanding the large deformations underwent by this specimen and the delamination of some layers of timber, the strains recorded in the timber revealed that the stresses remained within the elastic range.

These findings indicate that the failure of the tested STC beams is governed by plasticization of the steel section at midspan and at the joint sections where the slabs have a transversal discontinuity. The presence of these discontinuities (i.e. gaps filled with mortar) creates two additional critical sections where stresses tend to concentrate when certain load level is reached, due to the system's inability to transfer tensile forces through the gaps. The large deformations of the system and the concentration of the stresses at the gaps ultimately lead to the fracture of the mortar and delamination of the LVL slabs.

6. Conclusions and outlook

The construction sector needs sustainable solutions to reduce their carbon footprint and optimize the use of resources. Steel-timber composite beams for flooring systems are a relatively new solution that can be an alternative to carbon-intensive flooring systems such as steel-concrete composite floors and concrete floors.

This study introduces an innovative demountable and reusable steel-timber composite floor, implementing novel shear connections to connect timber slabs and steel beams. The STC flooring system exhibits significant promise for modularization, standardization, and off-site serial production, making it ideal for prefabrication in standard sizes and modules. Moreover, this flooring system offers the possibility to create spaces for adaptation and reconfiguration. The structure can be relocated, or individual structural components can be used in different buildings. Hence, it brings both environmental and economic benefits, and contributes to the transition of the construction sector towards the circular economy.

A similar SCC demountable and reusable system was developed in the REDUCE [81] project, and implemented in a demo project, the details have been thoroughly described by Odenbreit et al. [82,83]. The system proposed in this investigation is similar, however, it distinguishes itself by employing timber slabs instead of concrete slabs, alongside novel shear connections designed for easy demountability and

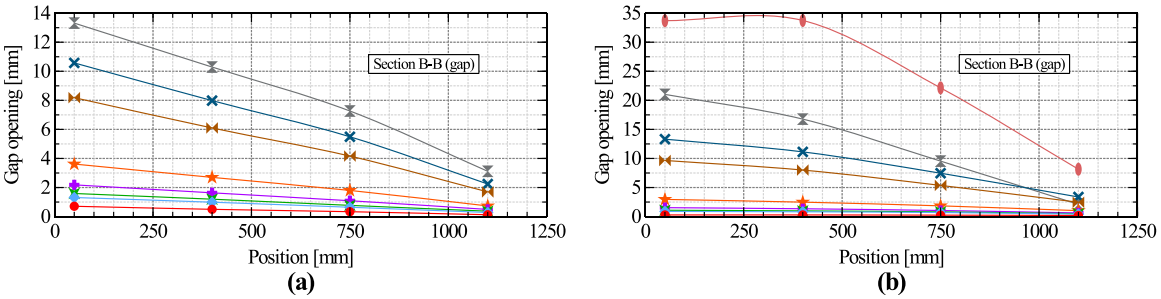

Fig. 20. Gap opening measured in section B-B at different loading stages for: (a) BT-1 and (b) BT-2, see the legend in Fig. 16 Fig. 18.

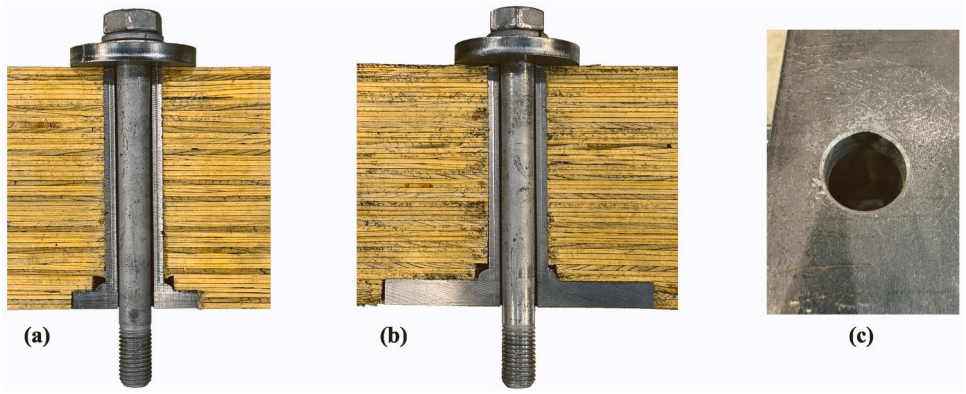

Fig. 21. (a) longitudinal cutting of the last connector (SCT-1) from BT-1; (b) longitudinal cutting of the last connector (SCT-3) from BT-2; (c) hole of a steel beam after the test.

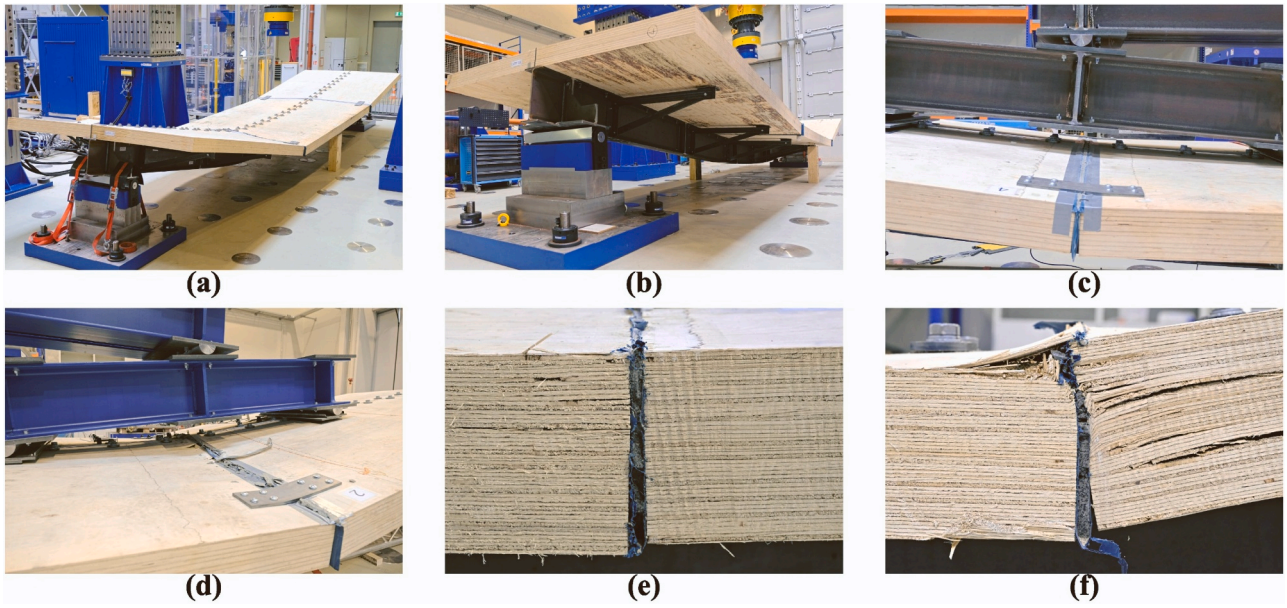

Fig. 22. Pictures taken after the test: (a) beam specimen from top; (b) beam specimen from below; (c) undamaged panel-to-panel gap of BT-1; (d) damaged panel-to-panel gap of BT-2; (e) cutting of undamaged gap; (f) cutting of damaged gap.

reuse. These systems contribute to decarbonization of the construction sector by allowing for the reuse of structural components, which in turn can reduce the demand for new materials and the associated emissions from their production chain. Moreover, the adoption of wood, which sequesters CO_2, significantly lowers the embodied carbon of constructions.Nevertheless, the supply of timber might not meet market demand. Therefore, combining timber with other materials such as steel and reusing these elements can help to mitigate timber shortage and reduce the need for new components.

The findings from the experimental six-point bending tests on STC beams with newly developed shear connections, have yielded several key insights, allowing to draw the following conclusions:

- The beams demonstrated substantial load-bearing and deformation capabilities. The tests were stopped due to the specimens reaching the maximum deformation given by the testing setup, nevertheless, the deformations reached in BT-1 and BT-2 were quite large, approximately 400 mm and 650 mm, respectively, and the maximum recorded loads were 674 kN (bending moment of 1011 kN·m) for BT-1, and 686 kN (bending moment of 1029 kN·m) for BT-2.
- The elastic limit of the two STC beams was reached at a load of approximately 400 kN (bending moment of 600 kN·m) and a mid-span deflection of 60 mm.
- It is common practice to consider that composite beams (e.g. SCC beams) have a good ductility when they can withstand deformations of at least $\ell/50$. In the STC beams tested in this investigation the maximum bending moment was reached at larger deformations, approximately $\ell/20$, indicating that these beams have good ductility.
- The shear connectors exhibited slip values smaller than 1 mm, for loads within the elastic range of the STC beams. This indicates that when loads remain within the elastic range (e.g. service conditions) it is possible to reuse the panels.
- Maximum slip values of 5.3 mm and 6.6 mm were recorded for BT-1 and BT-2, respectively. Indicating that even at large deformations, the connections are able to limit the slip, ensuring effective composite action and demonstrating their robustness.
- At the end of the test, the most stressed connections were cut longitudinally to assess the damages and nearly no damage was observed, only slight embedment of the shear connection devices in the timber with a permanent deformation of approximately 1 mm,

additionally, no deformations or damages were observed in the bolts and the holes of the flange of the steel beam.

- The steel beams in both specimens exhibited plasticization and underwent large deformations, yet without local damages or fracture. In BT-1 the largest recorded tensile strains in the bottom flange of the steel beams was at the midspan section. In BT-2 the steel beam exhibited a redistribution of stresses, the most stressed region was initially at midspan, from a certain loading stage little increase of strains was observed in the bottom flange of the steel beam in the midspan section whereas in the region near the transversal gap, the strains increased to large values. Thus, showing that the regions of the steel beam near the transversal gap plasticized to a larger extent than the midspan section, which is typically the most stressed in simply supported beams in sagging bending.
- The strength and failure of the STC beams was in both cases governed by the yielding and ultimate strength of the steel beam. Critical in this system are the regions near the transversal gaps as the tensile stresses in the steel beam tend to be larger in this region at large deformations. This means that, increasing the steel grade can enhance the utilization of the LVL slab and shift the yielding of the steel beam in the critical regions.
- The strains recorded in the timber remained within the elastic range, furthermore, the strain distribution through the width of the slab was not uniform, which indicates that the shear lag effects are to be considered. The effective width at midspan, estimated at the last loading stage was 1881 mm for BT-1 and 1771 mm for BT-2, corresponding to an effective width of approximately $\ell/5.5$.
- The use of high strength mortar to fill the transversal gaps was effective to transfer compression forces from the central panels to the edge panels, hence, the shear connectors of the edge panels were activated. Moreover, the mortar showed minimal damage despite significant deformations, in both tests it remained undamaged up to the loading stage VIII.
- BT-2 exhibited mortar crushing and LVL delamination near the transverse gaps post significant load, indicating that at large deformations these regions become potential points of failure. However, dividing the slabs along the longitudinal directions and having gaps between them is needed as it provides tolerances and facilitates transport and assembly / disassembly, which can be critical for long spans.

While these findings enhance our understanding of this structural system, the experimental campaign had constrains including: the implementation of only two types of connections, the testing of just one specimen for each shear connection type, the LVL slabs used had a thickness of 144 mm with their grain oriented parallel to the beam's longitudinal direction, only beams with a 10 m span and a slab width of 2.51 m were tested, the use of IPE 400 steel profiles in both cases and a steel grade of S355, among others. Given these limitations, further research is essential to expand the applicability of the results. Future investigations could explore various aspects, such as different types of connections, arrangements of connections, variations in LVL thickness and orientation, different spans and slab widths, alternative steel profiles and steel grades, and the use of other timber products like CLT. Such studies would deepen our understanding of STC beams.

Currently, there are no established technical standards for the structural design of composite structures like STC beams. Therefore, extensive research is essential to build a comprehensive knowledge database and develop robust design methodologies. This study contributes to this effort by presenting results from STC beams with novel shear connections, showcasing their significant potential for reuse. Ongoing work is focusing on the design of the STC beams. The design procedures build upon the concepts presented by Kozma [92] regarding shear connection considerations, and the analytical procedures to estimate the bending capacity of the STC beams are two: (i) a strain-controlled analysis of the critical cross sections, and (ii) a simplified analytical procedure. A detailed exposition of these analytical procedures and further details of this research can be found in [93].

Funding

This research and the APC were funded by Fonds National de la Recherche Luxembourg (FNR) and PREFALUX, and supported by ArcelorMittal Luxembourg, within the framework of the research project ''Prefa-SeTi: Steel-Timber Composite Beams'', Grant No. 15695062.

CRediT authorship contribution statement

Christoph Odenbreit: Methodology, Funding acquisition, Conceptualization, Project administration, Resources, Supervision, Writing – review & editing. **Alfredo Romero:** Writing – review & editing, Writing – original draft, Visualization, Validation, Software, Resources, Project administration, Methodology, Investigation, Funding acquisition, Formal analysis, Data curation, Conceptualization.

Declaration of Competing Interest

The authors declare the following financial interests/personal relationships which may be considered as potential competing interests: Alfredo Romero reports financial support and article publishing charges were provided by Fonds National de la Recherche (FNR). Alfredo Romero reports financial support was provided by PREFALUX. If there are other authors, they declare that they have no known competing financial interests or personal relationships that could have appeared to influence the work reported in this paper.

Data availability

Data are contained within the article.

Acknowledgements

The authors gratefully acknowledge the Luxembourg's National Research Fund (FNR), Prefalux, ArcelorMittal and MetsäWood for their support in the research project "Prefa-SeTi: Steel-Timber Composite Beams" (PhD Industrial Fellowship Grant No. 15695062). The authors wish to thank also the laboratory team (Gilbert Klein, Marc Seil, Ed Weyer, Mehdi Saeidi and Cyrille Inglebert) and the former student Gabriel Ibosiola for their support in this testing campaign.

References

[1] D'Amico B, Pomponi F, Hart J. Global Potential For Material Substitution In Building Construction: The Case Of Cross Laminated Timber. J Clean Prod 2021; 279:123487. https://doi.org/10.1016/j.jclepro.2020.123487.
[2] Abed J, Rayburg S, Rodwell J, Neave M. A Review of the Performance and Benefits of Mass Timber as an Alternative to Concrete and Steel for Improving the Sustainability of Structures. Sustainability 2022;14:5570. https://doi.org/10.3390/su14095570.
[3] Simonsen M, Kjønaas OJ, Aall C. Substitution of Fossil-Energy Intensive Building Materials by Wood Products – Does It Matter? A Case Study from Western Norway. J Clean Prod 2023;383:134941. https://doi.org/10.1016/j.jclepro.2022.134941.
[4] Asiz A, Smith I. Connection System of Massive Timber Elements Used in Horizontal Slabs of Hybrid Tall Buildings. J Struct Eng 2011;137. https://doi.org/10.1061/(asce)st.1943-541x.0000363.
[5] Loss C, Piazza M, Zandonini R. Connections for Steel–Timber Hybrid Prefabricated Buildings. Part I: Experimental Tests. Constr Build Mater 2016;122. https://doi.org/10.1016/j.conbuildmat.2015.12.002.
[6] Hassanieh A, Valipour HR, Bradford MA. Load-Slip Behaviour of Steel-Cross Laminated Timber (CLT) Composite Connections. J Constr Steel Res 2016;122. https://doi.org/10.1016/j.jcsr.2016.03.008.
[7] Hassanieh A, Valipour HR, Bradford MA. Experimental and Analytical Behaviour of Steel-Timber Composite Connections. Constr Build Mater 2016;118. https://doi.org/10.1016/j.conbuildmat.2016.05.052.
[8] Hassanieh A, Valipour HR, Bradford MA. Composite Connections between CLT Slab and Steel Beam: Experiments and Empirical Models. J Constr Steel Res 2017;138. https://doi.org/10.1016/j.jcsr.2017.09.002.

[9] Hassanieh A, Valipour HR, Bradford MA, Sandhaas C. Modelling of Steel-Timber Composite Connections: Validation of Finite Element Model and Parametric Study. Eng Struct 2017;138:35–49. https://doi.org/10.1016/j.engstruct.2017.02.016.

[10] Hassanieh A, Valipour HR, Bradford MA. Bolt Shear Connectors in Grout Pockets: Finite Element Modelling and Parametric Study. Constr Build Mater 2018;176. https://doi.org/10.1016/j.conbuildmat.2018.05.029.

[11] Yang R, Li H, Lorenzo R, Ashraf M, Sun Y, Yuan Q. Mechanical Behaviour of Steel Timber Composite Shear Connections. Constr Build Mater 2020;258. https://doi.org/10.1016/j.conbuildmat.2020.119605.

[12] Wang CL, Lyu J, Zhao J, Yang H. Experimental Investigation of the Shear Characteristics of Steel-to-Timber Composite Joints with Inclined Self-Tapping Screws. Eng Struct 2020;215. https://doi.org/10.1016/j.engstruct.2020.110683.

[13] Zhao Y, Yuan Y, Wang CL, Zheng J, Zhou Y. Experimental Study on Shear Performance of Steel-Timber Screw Connectors with Grout Pockets. Eng Struct 2022;266:114535. https://doi.org/10.1016/J.ENGSTRUCT.2022.114535.

[14] Moritani, F.Y.; Santos, P.; Jorge, L.; Dias, A. ANALYTICAL AND EXPERIMENTAL STUDY ON REVERSIBLE STEEL-TIMBER COMPOSITE CONNECTION SYSTEMS. In Proceedings of the World Conference on Timber Engineering (WCTE 2023); World Conference on Timber Engineering (WCTE 2023): Oslo, Norway, 2023; pp. 3364–3372.

[15] Gao Y, Xu F, Meng X, Zhang Y, Yang H. Experimental and Numerical Study on the Lateral Torsional Buckling of Full-Scale Steel-Timber Composite Beams. Adv Struct Eng 2022;25:522–40. https://doi.org/10.1177/13694332211057263.

[16] Chybiński M, Polus Ł. Experimental and Numerical Investigations of Aluminium-Timber Composite Beams with Bolted Connections. Structures 2021;34:1942–60. https://doi.org/10.1016/j.istruc.2021.08.111.

[17] Chybiński M, Polus Ł. Mechanical Behaviour of Aluminium-Timber Composite Connections with Screws and Toothed Plates. Materials 2022:*15*. https://doi.org/10.3390/ma15010068.

[18] Zhou Y, Zhao Y, Wang C-L, Zhou Y, Zheng J. Experimental Study of the Shear Performance of H-Shaped Aluminum-Timber Composite Connections. Constr Build Mater 2022;334:127421. https://doi.org/10.1016/j.conbuildmat.2022.127421.

[19] Zhang H, Ling Z. Finite Element Modeling on Shear Performance of Grouted Stud Connectors for Steel–Timber Composite Beams. Materials 2022;15:1196. https://doi.org/10.3390/ma15031196.

[20] Shulman S, Loss C. High-Performance Grout-Reinforced Shear Connectors for Hybrid Steel-Cross-Laminated Timber Building Systems: Experimental Study. J Build Eng 2023;67:106014. https://doi.org/10.1016/j.jobe.2023.106014.

[21] Romero, A.; Yang, J.; Hanus, F.; Degée, H.; Odenbreit, C. PUSH-OUT TESTS ON CONNECTIONS FOR DEMOUNTABLE AND REUSABLE STEEL-TIMBER COMPOSITE BEAM AND FLOORING SYSTEMS. In Proceedings of the World Conference on Timber Engineering (WCTE 2023); World Conference on Timber Engineering (WCTE 2023): Oslo, Norway, 2023; pp. 3568–3574.

[22] Böhm N, Vogelsberg A, Kühn B. Investigations of the Shear Connectors and the Load-bearing Behaviour of Steel Cross-laminated Timber Composite Beams. ce Pap 2023;6:78–83. https://doi.org/10.1002/cepa.2379.

[23] Loss C, Piazza M, Zandonini R. Connections for Steel–Timber Hybrid Prefabricated Buildings. Part II: Innovative Modular Structures. Constr Build Mater 2016;122. https://doi.org/10.1016/j.conbuildmat.2015.12.001.

[24] Ataei A, Chiniforush AA, Bradford M, Valipour H. Cyclic Behaviour of Bolt and Screw Shear Connectors in Steel-Timber Composite (STC) Beams. J Constr Steel Res 2019;161. https://doi.org/10.1016/j.jcsr.2019.05.048.

[25] Ataei A, Chiniforush AA, Bradford MA, Valipour HR, Ngo TD. Behaviour of Embedded Bolted Shear Connectors in Steel-Timber Composite Beams Subjected to Cyclic Loading. J Build Eng 2022;54:104581. https://doi.org/10.1016/j.jobe.2022.104581.

[26] European Committee for Standardisation CEN EN 1998–1:2004 - Eurocode 8: Design of Structures for Earthquake Resistance - Part 1: General Rules, Seismic Actions and Rules for Buildings 2004.

[27] Asiz A, Smith I. Demands Placed on Steel Frameworks of Tall Buildings Having Reinforced Concrete or Massive Wood Horizontal Slabs. Struct Eng Int 2009;19:395–403. https://doi.org/10.2749/101686609789847000.

[28] Hassanieh A, Valipour HR, Bradford MA. Experimental and Numerical Study of Steel-Timber Composite (STC) Beams. J Constr Steel Res 2016;122:367–78. https://doi.org/10.1016/j.jcsr.2016.04.005.

[29] Hassanieh A, Valipour HR, Bradford MA. Experimental and Numerical Investigation of Short-Term Behaviour of CLT-Steel Composite Beams. Eng Struct 2017;144. https://doi.org/10.1016/j.engstruct.2017.04.052.

[30] Loss C, Davison B. Innovative Composite Steel-Timber Floors with Prefabricated Modular Components. Eng Struct 2017;132. https://doi.org/10.1016/j.engstruct.2016.11.062.

[31] Owolabi D, Loss C. Experimental and Numerical Study on the Bending Response of a Prefabricated Composite CLT-Steel Floor Module. Eng Struct 2022;260:114278. https://doi.org/10.1016/j.engstruct.2022.114278.

[32] Böhm N, Vogelsberg A, Kühn B. Bending and Vibration Behaviour of CLT-Steel Composite Beams. sace 2024;34:75–88. https://doi.org/10.5755/j01.sace.34.1.35467.

[33] Zhao Y, Yuan Y, Wang C-L, Meng S. Experimental and finite element analysis of flexural performance of steel-timber composite beams connected by hybrid-anchored screws. Engineering Structures 2023;292:116503. https://doi.org/10.1016/j.engstruct.2023.116503.

[34] Keipour, N.; Valipour, H.R.; Bradford, M.A. Steel-Timber versus Steel-Concrete Composite Floors: A Numerical Study. In Proceedings of the WCTE 2016 - World Conference on Timber Engineering; 2016.

[35] Heinisuo M, Mela K, Pajunen S, Malaska M. NEW STEEL-TIMBER COMPOSITE BEAM, NORDIC SYSTEM. ce/Pap 2019;3. https://doi.org/10.1002/cepa.1194.

[36] Romero A, Yang J, Hanus F, Odenbreit C. Numerical Investigation of Steel-LVL Timber Composite Beams. ce Pap 2022;5:21–30. https://doi.org/10.1002/cepa.1694.

[37] Aspila A, Heinisuo M, Mela K, Malaska M, Pajunen S. Elastic Design of Steel-Timber Composite Beams. Wood Mater Sci Eng 2022;17:243–52. https://doi.org/10.1080/17480272.2022.2093128.

[38] Strzelecka J, Polus Ł, Chybiński M. Theoretical and Numerical Analyses of Steel-Timber Composite Beams with LVL Slabs. Civ Environ Eng Rep 2023;33:64–84. https://doi.org/10.59440/ceer/172510.

[39] Romero A, Yang J, Odenbreit C. Bending Resistance of Steel-timber Composite (STC) Beams: Analytical vs. Numerical Investigations. ce Pap 2023;6:59–64. https://doi.org/10.1002/cepa.2417.

[40] Möhler, K. Über Das Tragverhalten von Biegeträgern Und Druckstäben Mit Zusammengesetzten Querschnitten Und Nachgiebigen Verbindungsmitteln. Doctoral dissertation, 1956.

[41] European Committee for Standardisation CEN EN 1995–1-1:2004 - Eurocode 5: Design of Timber Structures - Part 1–1: General - Common Rules and Rules for Buildings 2004.

[42] European Committee for Standardisation CEN EN 1994–1-1:2004 - Design of Composite Steel and Concrete Structures - Part 1–1: General Rules and Rules for Buildings 2004.

[43] Keipour N, Valipour HR, Bradford MA. Steel-Timber Composite Beam-to-Column Joints: Effect of Connections between Timber Slabs. J Constr Steel Res 2018;151. https://doi.org/10.1016/j.jcsr.2018.09.019.

[44] Keipour N, Valipour HR, Bradford MA. Experimental Study of Steel-Timber Composite (STC) Beam to Steel Column Joints Having a Flush End-Plate. Eng Struct 2018;174. https://doi.org/10.1016/j.engstruct.2018.08.009.

[45] Nouri F, Bradford M, Valipour H. Steel–Timber Composite Beam-to-Column Connections with Shear Tab. J Struct Eng 2019;145. https://doi.org/10.1061/(asce)st.1943-541x.0002274.

[46] Ataei A, Valipour HR, Bradford MA, Chiniforush AA. Experimental Study of Steel-Timber Composite Beam-to-Column Joints with Extended End Plates. Constr Build Mater 2019;226. https://doi.org/10.1016/j.conbuildmat.2019.07.154.

[47] Nouri F, Valipour HR. Semi-Rigid Partial-Strength Steel-Timber Composite (STC) Connections with Mechanically Anchored Steel Rods. J Constr Steel Res 2019;158. https://doi.org/10.1016/j.jcsr.2019.04.017.

[48] Nouri F, Valipour HR, Bradford MA. Finite Element Modelling of Steel-Timber Composite Beam-to-Column Joints with Nominally Pinned Connections. Eng Struct 2019;201. https://doi.org/10.1016/j.engstruct.2019.109854.

[49] Nouri F, Valipour HR, Bradford MA. Structural Behaviour of Steel-Timber Composite (STC)Beam-to-Column Connections with Double Angle Web Cleats Subjected to Hogging Bending Moment. Eng Struct 2019;192. https://doi.org/10.1016/j.engstruct.2019.04.092.

[50] Nouri F, Valipour HR. Moment-Rotation Model for Steel-Timber Composite Connections with Slab Continuity Steel Rods. J Constr Steel Res 2020;173. https://doi.org/10.1016/j.jcsr.2020.106257.

[51] Keipour N, Valipour HR, Bradford MA. Structural Behaviour of Steel-Timber versus Steel-Concrete Composite Joints with Flush End Plate. Constr Build Mater 2020;262. https://doi.org/10.1016/j.conbuildmat.2020.120885.

[52] Qazizadeh S, Hashemi SK, Valipour HR. Numerical Investigation of Steel-Timber Composite Floors with Flush End-Plate Connection. Structures 2023;56:104892. https://doi.org/10.1016/j.istruc.2023.104892.

[53] Chiniforush AA, Valipour HR, Bradford MA, Akbarnezhad A. Long-Term Behaviour of Steel-Timber Composite (STC) Shear Connections. Eng Struct 2019;196. https://doi.org/10.1016/j.engstruct.2019.109356.

[54] Chiniforush AA, Valipour HR, Akbarnezhad A. Long-Term Coupled Analysis of Steel-Timber Composite (STC) Beams. Constr Build Mater 2021;278:122348. https://doi.org/10.1016/j.conbuildmat.2021.122348.

[55] Chiniforush AA, Valipour HR, Bradford MA, Akbar Nezhad A. Experimental and Theoretical Investigation of Long-Term Performance of Steel-Timber Composite Beams. Eng Struct 2021;249:113314. https://doi.org/10.1016/j.engstruct.2021.113314.

[56] Chiniforush AA, Valipour H, Akbarnezhad A, Bradford M. 08.27: Steel-timber Composite (STC) Beams: Numerical Simulation of Long-term Behaviour. ce Pap 2017;1:2051–9. https://doi.org/10.1002/cepa.250.

[57] Chiniforush, A.A.; Akbarnezhad, A.; Malek, S. Time-Dependent Deflection Measurement for Steel-Timber Composite (STC) Flooring System. In Proceedings of the International Conference on Advances in Experimental Structural Engineering; 2020; Vol. 2020-February.

[58] Chiniforush, A.A.; Akbarnezhad, A.; Valipour, H.; Dackermann, U. DYNAMIC RESPONSE OF STEEL-TIMBER COMPOSITE (STC) BEAMS. In Proceedings of the Proceedings of the 24th International Congress on Sound and Vibration; London, UK, 2017.

[59] A. Chiniforush A, Makki Alamdari M, Dackermann U, Valipour HR, Akbarnezhad A. Vibration Behaviour of Steel-Timber Composite Floors, Part (1): Experimental & Numerical Investigation. J Constr Steel Res 2019;161. https://doi.org/10.1016/j.jcsr.2019.07.007.

[60] Hassanieh A, Chiniforush AA, Valipour HR, Bradford MA. Vibration Behaviour of Steel-Timber Composite Floors, Part (2): Evaluation of Human-Induced Vibrations. J Constr Steel Res 2019;158. https://doi.org/10.1016/j.jcsr.2019.03.026.

[61] Huang H, Gao Y, Chang W-S. Human-Induced Vibration of Cross-Laminated Timber (CLT) Floor under Different Boundary Conditions. Eng Struct 2020;204:110016. https://doi.org/10.1016/j.engstruct.2019.110016.

[62] Wang C, Chang W-S, Yan W, Huang H. Predicting the Human-Induced Vibration of Cross Laminated Timber Floor under Multi-Person Loadings. Structures 2021;29:65–78. https://doi.org/10.1016/j.istruc.2020.10.074.

[63] Cheraghi-Shirazi N, Crews K, Malek S. Review of Vibration Assessment Methods for Steel-Timber Composite Floors. Buildings 2022;12:2061. https://doi.org/10.3390/buildings12122061.
[64] Karampour H, Piran F, Faircloth A, Talebian N, Miller D. Vibration of Timber and Hybrid Floors: A Review of Methods of Measurement, Analysis, and Design. Buildings 2023;13:1756. https://doi.org/10.3390/buildings13071756.
[65] Owolabi, D.; Loss, C. EXPERIMENTAL STUDY ON THE VIBRATION CHARACTERISTICS OF A PREFABRICATED CROSS-LAMINATED TIMBER-STEEL COMPOSITE FLOOR. In Proceedings of the World Conference on Timber Engineering (WCTE 2023); World Conference on Timber Engineering (WCTE 2023): Oslo, Norway, 2023; pp. 1880–1887.
[66] Owolabi D, Loss C, Zhou J. Vibration Properties and Serviceability Performance of a Modular Cross-Laminated Timber-Steel Composite Floor System. J Struct Eng 2023;149:04023171. https://doi.org/10.1061/JSENDH.STENG-12587.
[67] Zhang J, Zhang C, Li Y, Chang W-S, Huang H. Cross-Laminated Timber (CLT) Floor Serviceability under Multi-Person Loading: Impact of Beam–Panel Connections. Eng Struct 2023;296:116941. https://doi.org/10.1016/j.engstruct.2023.116941.
[68] Li Z, He M, Ma Z, Wang K, Ma R. In-Plane Behavior of Timber-Steel Hybrid Floor Diaphragms: Experimental Testing and Numerical Simulation. J Struct Eng 2016;142:04016119. https://doi.org/10.1061/(ASCE)ST.1943-541X.0001601.
[69] Loss C, Frangi A. Experimental Investigation on In-Plane Stiffness and Strength of Innovative Steel-Timber Hybrid Floor Diaphragms. Eng Struct 2017;138:229–44. https://doi.org/10.1016/j.engstruct.2017.02.032.
[70] Loss C, Rossi S, Tannert T. In-Plane Stiffness of Hybrid Steel–Cross-Laminated Timber Floor Diaphragms. J Struct Eng 2018;144:04018128. https://doi.org/10.1061/(ASCE)ST.1943-541X.0002105.
[71] Chiniforush AA, Akbarnezhad A, Valipour H, Xiao J. Energy Implications of Using Steel-Timber Composite (STC) Elements in Buildings. Energy Build 2018. https://doi.org/10.1016/j.enbuild.2018.07.038.
[72] Hammad MW, Valipour HR, Ghanbari-Ghazijahani T, Bradford MA. Timber-Timber Composite (TTC) Beams Subjected to Hogging Moment. Constr Build Mater 2022;321:126295. https://doi.org/10.1016/j.conbuildmat.2021.126295.
[73] European Commission. Directorate General for Communication. European Green Deal: Delivering on Our Targets.; Publications Office: LU, 2021;
[74] United Nations Resolution Adopted by the General Assembly on 25 September 2015, Transforming Our World: The 2030 Agenda for Sustainable Development, UN Document: A/RES/70/1 (accessed on 26 January 2023).
[75] Romero A, Odenbreit C. Experimental Investigation on Novel Shear Connections for Demountable Steel-Timber Composite (STC) Beams and Flooring Systems. Eng Struct 2024;304:117620. https://doi.org/10.1016/j.engstruct.2024.117620.
[76] European Committee for Standardisation CEN EN 10025 - Hot Rolled Products for Structural Steels 2004.
[77] DIBt ETA-11/0190 - European Technical Assessment of Würth Self-Tapping Screws 2018.
[78] European Committee for Standardisation CEN EN 14399 - High-Strength Structural Bolting Assemblies for Preloading 2015.
[79] European Committee for Standardisation CEN EN 1993–1-8:2005 - Eurocode 3: Design of Steel Structures - Part 1–8: Design of Joints 2005.
[80] European Committee for Standardisation CEN EN 1090–2- Execution of Steel Structures and Aluminium Structures - Part 2: Technical Requirements for Steel Structures 2018.
[81] Sansom, M.; Girao Coelho, A.; Lawson, R.M.; Odenbreit, C.; Kozma, A.; Lam, D.; Dai, X.; Yang, J.; Oly, R.; Hoekstra Bobbema, B.; et al. Reuse and Demountability Using Steel Structures and the Circular Economy (REDUCE) 2020.
[82] Odenbreit C, Yang J, Kozma A, Romero A, Popa N, Hanus F, Obiala R. Design for Disassembling, Reuse, and the Circular Economy: A Demonstration Building, "Petite Maison. ce Pap 2023;6:369–73. https://doi.org/10.1002/cepa.2537.
[83] Odenbreit C, Yang J, Romero A, Kozma A. A Lego-like steel-framed system for standardization and serial production. Steel Constr 2023;16:56–64. https://doi.org/10.1002/stco.202200021.
[84] Metsä Wood Kerto ® LVL Q-Panel 2022.
[85] Chybiński M, Polus Ł. Experimental Study of Aluminium-Timber Composite Bolted Connections Strengthened with Toothed Plates. Materials 2022;15:5271. https://doi.org/10.3390/MA15155271.
[86] Finnish Woodworking Industries LVL Handbook ; Federation of the Finish Woodworking Industries: Helsinki, Finland, 2019; ISBN 978–952-94–2346-0.
[87] PAGEL Pagel Super High Strength Grout C100/115 (Technical Data Sheet) 2021.
[88] European Committee for Standardisation CEN EN ISO 6892–1 Metallic Materials - Tensile Testing (Part 1: Method of Test at Room Temperature) 2016.
[89] Romero A, Odenbreit C. Experimental Investigation on Strength and Stiffness Properties of Laminated Veneer Lumber (LVL). Materials 2023;16:7194. https://doi.org/10.3390/ma16227194.
[90] European Committee for Standardisation CEN EN 26891 - Timber Structures - Joints Made with Mechanical Fasteners - Gneral Principles for the Determination of Strength and Deformation Characteristics.
[91] Masoudnia R, Hashemi A, Quenneville P. Predicting the Effective Flange Width of a CLT Slab in Timber Composite Beams. J Struct Eng 2018;144:04018084. https://doi.org/10.1061/(ASCE)ST.1943-541X.0001979.
[92] Kleinhenz, M.; Viertel, M.; Demschner, T.; Frangi, A. Determination of the effective width of cross-laminated timber rib panels using digital image correlation. In Proceedings of the World Conference on Timber Engineering (WCTE 2023); World Conference on Timber Engineering (WCTE 2023): Oslo, Norway, 2023; pp. 2416–2425.
[93] Romero A. Demountable and Reusable Steel-Timber Composite Beams. Doctoral Thesis. University of Luxembourg; 2024.